

# Riemannian adaptive stochastic gradient algorithms on matrix manifolds

Hiroyuki Kasai\*

Pratik Jawanpuria<sup>†</sup>

Bamdev Mishra<sup>‡</sup>

July 1, 2019

## Abstract

Adaptive stochastic gradient algorithms in the Euclidean space have attracted much attention lately. Such explorations on Riemannian manifolds, on the other hand, are relatively new, limited, and challenging. This is because of the intrinsic non-linear structure of the underlying manifold and the absence of a canonical coordinate system. In machine learning applications, however, most manifolds of interest are represented as matrices with notions of row and column subspaces. In addition, the implicit manifold-related constraints may also lie on such subspaces. For example, the Grassmann manifold is the set of column subspaces. To this end, such a rich structure should not be lost by transforming matrices to just a stack of vectors while developing optimization algorithms on manifolds. We propose novel stochastic gradient algorithms for problems on Riemannian matrix manifolds by adapting the row and column subspaces of gradients. Our algorithms are provably convergent and they achieve the convergence rate of order  $\mathcal{O}(\log(T)/\sqrt{T})$ , where  $T$  is the number of iterations. Our experiments illustrate the efficacy of the proposed algorithms on several applications.

## 1 Introduction

Large-scale machine learning applications are predominantly trained using stochastic gradient descent (SGD) (Bottou et al., 2018) based algorithms today. A (sub)class of such algorithms that has become increasingly common lately adapts the learning rate of each coordinate of the gradient vector based on past iterates (McMahan & Streeter, 2010; Duchi et al., 2011). A key motivation for this is to have different learning rates for different coordinates (Zeiler, 2012; Pennington et al., 2014), a feature which vanilla SGD lacks. ADAM (Kingma & Ba, 2015), arguably the most popular adaptive gradient method, additionally employs a momentum term to modify the search direction as well. Adaptive gradient methods have enjoyed varying degrees of success in various applications (Pennington et al., 2014; Wilson et al., 2017; Zaheer et al., 2018; Shah et al., 2018).

In this paper, we focus on adaptive stochastic gradient algorithms on Riemannian manifolds. Riemannian geometry is a generalization of the Euclidean geometry (Lee, 2003). It includes several non-Euclidean spaces such as set of symmetric positive-definite matrices, and set of orthogonal matrices, to name a few. Numerous machine learning problems can be cast as an optimization problem on Riemannian manifolds. Examples include principal component analysis

---

\*The University of Electro-Communications, Japan (e-mail: kasai@is.uec.ac.jp)

<sup>†</sup>Microsoft, India (e-mail: pratik.jawanpuria@microsoft.com)

<sup>‡</sup>Microsoft, India (e-mail: bamdevm@microsoft.com)

(PCA), matrix completion (Vandereycken, 2013; Mishra & Sepulchre, 2014; Boumal & Absil, 2015b; Jawanpuria & Mishra, 2018), learning taxonomy or latent hierarchies (Nickel & Kiela, 2017, 2018; Ganea et al., 2018), deep metric learning (Harandi et al., 2017a), multi-task learning (Mishra et al., 2019), applications in computer vision (Kasai & Mishra, 2016; Harandi et al., 2017b; Nimishakavi et al., 2018), bilingual lexicon induction (Jawanpuria et al., 2019), among others. Several Euclidean algorithms, e.g., steepest descent, conjugate gradients, and trust-regions, have been generalized to Riemannian manifolds (Absil et al., 2008).

Bonnabel (2013) first proposed the Riemannian SGD (RSGD) algorithm, which is a generalization of the (Euclidean) SGD algorithm to Riemannian manifolds. However, such a generalization of Euclidean adaptive gradient algorithm is relatively unexplored. A key difficulty in this regard is the absence of a canonical coordinate system on manifolds and the inherent non-linear geometry of the manifold. Recent works in this direction compute Euclidean-style adaptive weights in the Riemannian setting, ignoring the geometry of the underlying manifold. Roy et al. (2018) propose a RMSProp-style algorithm for manifolds, viewing the gradient as a vector and computing a corresponding adaptive weight vector. On the other hand, Cho & Lee (2017); Bécigneul & Ganea (2019) adapt the step size by computing a scalar weight instead of directly adapting the gradient in a momentum-based Riemannian AMSGrad/ADAM-style algorithm.

We develop a novel approach of adapting the Riemannian gradient, which allows to exploit the structure of the underlying manifolds. In particular, we propose to adapt the row and column subspaces of the Riemannian stochastic gradient  $\mathbf{G}$ . Euclidean adaptive algorithms compute (positive) adaptive weight vectors for the gradient vectors. Our model computes *left* and *right* adaptive weight matrices for  $\mathbf{G}$  denoted by  $\mathbf{L}$  and  $\mathbf{R}$ , respectively.  $\mathbf{L}$  adapts the row subspace of  $\mathbf{G}$  and  $\mathbf{R}$  adapts the column subspace of  $\mathbf{G}$ . Both  $\mathbf{L}$  and  $\mathbf{R}$  are positive definite matrices and are computed using the row covariance and column covariance matrices of  $\mathbf{G}$ , respectively. For computational efficiency, we model  $\mathbf{L}$  and  $\mathbf{R}$  as diagonal matrices, taking cue from AdaGrad (Duchi et al., 2011). Overall, we propose computationally efficient Riemannian adaptive stochastic gradient algorithms, henceforth collectively termed as RASA.

Under a set of mild conditions, our analysis guarantees the convergence of our algorithms with a rate of convergence of order  $O(\log(T)/\sqrt{T})$ , where  $T$  is the number of iterations. To the best of our knowledge, ours is the first Riemannian adaptive gradient algorithm to provide convergence analysis for non-convex stochastic optimization setting. Among the existing works, Bécigneul & Ganea (2019) provide convergence analysis only for geodesically convex functions.

Empirically, we compare our algorithms with the existing Riemannian adaptive gradient algorithms. In applications such as principal components analysis and matrix completion, we observe that our algorithms perform better than the baselines in most experiments both on synthetic and real-world datasets.

The main contributions of this work are:

- we propose a principled approach for modeling adaptive weights for Riemannian stochastic gradient. We model adaptive weight matrices for row and column subspaces exploiting the geometry of the manifold.
- we develop efficient Riemannian adaptive stochastic gradient algorithms, based on the proposed modeling approach.
- we provide convergence analysis of our algorithm, under a set of mild conditions. Our algorithms achieve a rate of convergence order  $O(\log(T)/\sqrt{T})$ , where  $T$  is the number of iterations, for non-convex stochastic optimization.

The paper is organized as follows. Section 2 discusses preliminaries of the Riemannian (stochastic) optimization framework and adaptive stochastic gradient algorithms in the Euclidean space. In Section 3, we present our Riemannian adaptive stochastic algorithms. Section 4 provides the convergence analysis of the proposed algorithms. Related works are discussed in Section 5, while empirical results are presented in Section 6. Section 7 concludes the paper.

## 2 Preliminaries

In this section, we briefly summarize various concepts of Riemannian geometry and optimization. We refer the interested readers to (Absil et al., 2008) for more details.

### Notions on Riemannian manifolds

Informally, a manifold is a generalization of the notion of surface to higher dimensions. A manifold  $\mathcal{M}$  of dimension  $d$  can be locally approximated by  $\mathbb{R}^d$ . For example, the Stiefel manifold is the set of  $n \times r$  orthonormal matrices and has dimension  $d = np - p(p + 1)/2$  (Absil et al., 2008). The first order approximation of  $\mathcal{M}$  around a point  $x \in \mathcal{M}$  is a  $d$  dimensional vector space and is known as the tangent space  $T_x\mathcal{M}$ . The tangent space  $T_x\mathcal{M}$  contains all tangent vectors to  $\mathcal{M}$  at  $x$ . Corresponding to each tangent space  $T_x\mathcal{M}$ , we define an inner product  $g_x(\cdot, \cdot) : T_x\mathcal{M} \times T_x\mathcal{M} \rightarrow \mathbb{R}$ , which varies smoothly with  $x$ . This inner product is termed as the Riemannian metric in differential geometry. A Riemannian manifold comprises a manifold  $\mathcal{M}$  along with the collection of Riemannian metric  $g := (g_x)_{x \in \mathcal{M}}$ .

It should be noted that  $g_x$  induces a norm on the tangent space  $T_x\mathcal{M}$  at  $x$ :  $\|\xi\|_x = \sqrt{g_x(\xi, \xi)}$ , where  $\xi \in T_x\mathcal{M}$ . This in turn induces a (local) distance function on  $\mathcal{M}$ , which is employed to compute length of a path between two points on  $\mathcal{M}$ . A geodesic between two points is a path of shortest length on the manifold, generalizing the notion of straight line in Euclidean space to manifolds.

Minimizing an objective function  $f$  over the manifold  $\mathcal{M}$  requires the notion of gradients at every point  $x \in \mathcal{M}$ . Correspondingly, the Riemannian gradient  $\text{grad}f(x)$  at  $x \in \mathcal{M}$  is defined as an element of the tangent space  $T_x\mathcal{M}$ .

### Riemannian stochastic gradient update

The *Riemannian stochastic gradient descent* (RSGD) update (Bonnabel, 2013) is given by

$$x_{t+1} = R_{x_t}(-\alpha_t \text{grad}f_t(x_t)), \tag{1}$$

where  $\alpha_t > 0$  is a (decaying) step-size. The term  $\text{grad}f_i(x)$  represents a Riemannian stochastic gradient and is typically computed as the Riemannian gradient of the objective function on a batch of data  $y_i$ , *i.e.*,  $\text{grad}f_i(x) := \text{grad}f_i(x; y_i)$ . The retraction,  $R_x : T_x\mathcal{M} \rightarrow \mathcal{M} : \zeta \mapsto R_x(\zeta)$ , maps tangent space  $T_x\mathcal{M}$  onto  $\mathcal{M}$  with a local rigidity condition that preserves the gradients at  $x$  (Absil et al., 2008, Sec. 4.1). The exponential mapping is an instance of the retraction.

It should be noted that when the manifold is the Euclidean space ( $\mathcal{M} = \mathbb{R}^d$ ) and the Riemannian metric is the standard Euclidean inner product, the RSGD update (1) simplifies to the (vanilla) stochastic gradient descent (SGD) update (Bottou et al., 2018):

$$x_{t+1} = x_t - \alpha_t \nabla f_t(x_t), \tag{2}$$

where  $\nabla f_i(x)$  is a stochastic gradient commonly computed as the gradient of the objective function on a batch of data  $y_i$ , *i.e.*,  $\nabla f_i(x) = \nabla f_i(x; y_i)$ . The retraction function in the Euclidean space is given by  $R_x(z) = x + z$ .

### Euclidean adaptive stochastic gradient updates

The adaptive stochastic gradient methods employ the past gradients to compute a local distance measure and subsequently rescale the learning rate of each coordinate of the (Euclidean) model parameter. The AdaGrad algorithm (Duchi et al., 2011) introduced the following update, when  $x \in \mathbb{R}^d$ :

$$x_{t+1} = x_t - \alpha_t \mathbf{V}_t^{-1/2} \nabla f_t(x_t), \tag{3}$$

where  $\mathbf{V}_t$  is a diagonal matrix corresponding to the vector  $\mathbf{v}_t = \sum_{k=1}^t \nabla f_k(x_k) \circ \nabla f_k(x_k)$ , *i.e.*,  $\mathbf{V}_t = \text{Diag}(\mathbf{v}_t)$ , and the symbol ‘ $\circ$ ’ denotes the entry-wise product (Hadamard product). RMSProp (Tieleman & Hinton, 2012) proposed an exponentially moving average of the adaptive term  $\mathbf{v}_t$  as follows:  $\mathbf{v}_t = \beta \mathbf{v}_{t-1} + (1 - \beta) \nabla f_t(x_t) \circ \nabla f_t(x_t)$ , where  $\beta \in (0, 1)$  is another hyper-parameter.

Various stochastic gradient algorithms also employ an adaptive momentum term, ADAM (Kingma & Ba, 2015) being the most popular of them. In this paper, we restrict our discussion to algorithms *without* a momentum term because the calculation of the momentum term needs additional *vector transport operation* every iteration (Absil et al., 2008, Sec. 8.1). However, we include existing adaptive momentum based Riemannian stochastic gradient algorithms (Bécigneul & Ganea, 2019) as baselines in our experiments.

## 3 Riemannian adaptive stochastic gradient

In this section, we propose novel adaptive stochastic gradient algorithms in Riemannian setting. We first introduce a few notations, which will be useful in the rest of the manuscript. For given vectors  $\mathbf{a}$  and  $\mathbf{b}$ ,  $\sqrt{\mathbf{a}}$  or  $\mathbf{a}^{1/2}$  is element-wise square root,  $\mathbf{a}^2$  is element-wise square,  $\mathbf{a}/\mathbf{b}$  denotes element-wise division, and  $\max(\mathbf{a}, \mathbf{b})$  denotes element-wise maximum. For a given matrix  $\mathbf{A} \in \mathbb{R}^{n \times r}$ ,  $\text{vec}(\mathbf{A}) \in \mathbb{R}^{nr}$  denotes its vectorial representation. The term  $\mathbf{I}_d$  represents the identity matrix of  $d$  dimension.

We consider the following problem

$$\min_{x \in \mathcal{M}} f(x), \tag{4}$$

where elements of the manifold  $\mathcal{M}$  are represented as matrices of size  $n \times r$ . Such a geometry is true for most Riemannian manifolds employed in machine learning applications. Prominent examples of such manifolds include the Stiefel, Grassmann, spherical, symmetric positive definite, spectrahedron, and hyperbolic manifolds, to name a few.

In this paper, we are interested in a stochastic optimization setting where we assume that at each time step  $t$ , the algorithm computes a feasible point  $x_{t+1} \in \mathcal{M}$  given the current iterate  $x_t \in \mathcal{M}$ . For simplicity, the Riemannian stochastic gradient  $\text{grad} f_t(x_t) \in \mathbb{R}^{n \times r}$  at a given iterate  $x_t$  is denoted by  $\mathbf{G}_t$ . We exploit the matrix structure of  $\mathbf{G}_t$  by proposing separate adaptive weight *matrices* corresponding to row and column subspaces with  $\mathbf{L}_t \in \mathbb{R}^{n \times n}$  and  $\mathbf{R}_t \in \mathbb{R}^{r \times r}$ , respectively. These weights are computed in an exponentially weighted manner as

$$\begin{aligned} \mathbf{L}_t &= \beta \mathbf{L}_{t-1} + (1 - \beta) \mathbf{G}_t \mathbf{G}_t^\top / r, \\ \mathbf{R}_t &= \beta \mathbf{R}_{t-1} + (1 - \beta) \mathbf{G}_t^\top \mathbf{G}_t / n, \end{aligned} \tag{5}$$

where  $\beta \in (0, 1)$  is a hyper-parameter. It should be noted that  $\mathbf{G}_t \mathbf{G}_t^\top / r$  and  $\mathbf{G}_t^\top \mathbf{G}_t / n$  correspond to row and column covariance matrices, respectively. We propose to *adapt*<sup>1</sup> the Riemannian gradient  $\mathbf{G}_t$  as

$$\tilde{\mathbf{G}}_t = \mathbf{L}_t^{-1/4} \mathbf{G}_t \mathbf{R}_t^{-1/4}. \quad (6)$$

We observe that  $\mathbf{L}_t$  and  $\mathbf{R}_t$  weight matrices suitably modify the Riemannian gradient  $\mathbf{G}_t$  while respecting the matrix structure of  $\mathbf{G}_t$ , rather than plainly viewing  $\mathbf{G}_t$  as a vector in  $\mathbb{R}^{nr}$ . For instance in the Grassmann manifold, our right adaptive weight matrix  $\mathbf{R}_t$  essentially provides different learning rates to different column subspaces instead of giving different learning rates to the individual entries (coordinates) of  $\mathbf{G}_t$ . Our framework allows adapting only the row or the column space of  $\mathbf{G}_t$  as well by simply substituting  $\mathbf{R}_t = \mathbf{I}_r$  or  $\mathbf{L}_t = \mathbf{I}_n$ , respectively. In vectorial representation, the adaptive update (6) may be viewed as

$$\text{vec}(\tilde{\mathbf{G}}_t) = \mathbf{V}_t^{-1/2} \text{vec}(\mathbf{G}_t). \quad (7)$$

where  $\mathbf{V}_t = \mathbf{R}_t^{1/2} \otimes \mathbf{L}_t^{1/2}$ .

It should be noted that  $\tilde{\mathbf{G}}_t$  does not lie on the tangent plane  $T_{x_t} \mathcal{M}$ . Hence, the proposed adaptive Riemannian gradient is  $\mathcal{P}_{x_t}(\tilde{\mathbf{G}}_t)$ , where  $\mathcal{P}_x$  is a linear operator to project onto the tangent space  $T_x \mathcal{M}$ . Overall, the proposed update is

$$x_{t+1} = R_{x_t}(-\alpha_t \mathcal{P}_{x_t}(\tilde{\mathbf{G}}_t)), \quad (8)$$

where  $\tilde{\mathbf{G}}_t$  is defined as in (6).

**Remark 1:** The following generalization of the proposed adaptation of the Riemannian gradient (6) is permissible within our framework:

$$\tilde{\mathbf{G}}_t = \mathbf{L}_t^{-1/p} \mathbf{G}_t \mathbf{R}_t^{-1/q}. \quad (9)$$

where  $1/p + 1/q = 1/2$  and  $p, q > 0$ . For clarity in exposition, we choose  $p = q = 4$  in the remainder of the paper, including the experiment section. The proposed theoretical results (discussed in Section 4) hold for other permissible values of  $p$  and  $q$  as well.

## Diagonal adaptation and the proposed algorithm

The proposed *full* matrix update (8) is computationally prohibitive for high dimensional data. Hence, taking cue from the Euclidean adaptive gradient algorithms (Duchi et al., 2011), we propose diagonal adaptation of adaptive weight matrices. In particular, we model  $\mathbf{L}_t$  and  $\mathbf{R}_t$  as diagonal matrices corresponding to vectors  $\mathbf{l}_t \in \mathbb{R}^n$  and  $\mathbf{r}_t \in \mathbb{R}^r$ , which are computed as

$$\begin{aligned} \mathbf{l}_t &= \beta \mathbf{l}_{t-1} + (1 - \beta) \text{diag}(\mathbf{G}_t \mathbf{G}_t^\top), \\ \mathbf{r}_t &= \beta \mathbf{r}_{t-1} + (1 - \beta) \text{diag}(\mathbf{G}_t^\top \mathbf{G}_t), \end{aligned} \quad (10)$$

where the function  $\text{diag}(\cdot)$  returns the diagonal vector of a square matrix. The diagonal adaptation significantly reduces the effective dimension of adaptive weights to  $n + r$  and the computational complexity of adapting  $\mathbf{G}_t \in \mathbb{R}^{n \times r}$  with (diagonal) weight matrices to  $O(nr)$ .

---

<sup>1</sup>For numerical stability while computing square root of  $\mathbf{L}_t$  and  $\mathbf{R}_t$  in (6), a small  $\epsilon = 10^{-8}$  is added to their diagonal entries.

---

**Algorithm 1** Riemannian adaptive stochastic algorithm

---

**Require:** Step size  $\{\alpha_t\}_{t=1}^T$ , hyper-parameter  $\beta$ .

- 1: Initialize  $x_1 \in \mathcal{M}$ ,  $\mathbf{l}_0 = \hat{\mathbf{l}}_0 = \mathbf{0}_n$ ,  $\mathbf{r}_0 = \hat{\mathbf{r}}_0 = \mathbf{0}_r$ .
- 2: **for**  $t = 1, 2, \dots, T$  **do**
- 3:   Compute Riemannian stochastic gradient  $\mathbf{G}_t = \text{grad}f_t(x_t)$ .
- 4:   Update  $\mathbf{l}_t = \beta\mathbf{l}_{t-1} + (1 - \beta)\text{diag}(\mathbf{G}_t\mathbf{G}_t^T)/r$ .
- 5:   Calculate  $\hat{\mathbf{l}}_t = \max(\hat{\mathbf{l}}_{t-1}, \mathbf{l}_t)$ .
- 6:   Update  $\mathbf{r}_t = \beta\mathbf{r}_{t-1} + (1 - \beta)\text{diag}(\mathbf{G}_t^T\mathbf{G}_t)/n$ .
- 7:   Calculate  $\hat{\mathbf{r}}_t = \max(\hat{\mathbf{r}}_{t-1}, \mathbf{r}_t)$ .
- 8:    $x_{t+1} = R_{x_t}(-\alpha_t\mathcal{P}_{x_t}(\text{Diag}(\hat{\mathbf{l}}_t^{-1/4})\mathbf{G}_t\text{Diag}(\hat{\mathbf{r}}_t^{-1/4})))$ .
- 9: **end for**

---

The final algorithm is summarized in Algorithm 1 and is henceforth referred to as RASA (**R**iemannian **A**daptive **S**tochastic gradient **A**lgorithm on matrix manifolds). RASA generalizes Euclidean AdaGrad-type and RMSProp-type algorithms to Riemannian matrix manifolds.

We employ  $\hat{\mathbf{l}}_t = \max(\hat{\mathbf{l}}_{t-1}, \mathbf{l}_t)$  and  $\hat{\mathbf{r}}_t = \max(\hat{\mathbf{r}}_{t-1}, \mathbf{r}_t)$  in our final update (step 8, Algorithm 1). The non-decreasing sequence of the adaptive weights (along with non-increasing sequence of step size  $\alpha_t$ ) ensures the convergence of RASA. Such a sequence for adaptive weights was introduced by Reddi et al. (2018) in ADAM to provide convergence guarantees. We present our convergence analysis of Algorithm 1 in Section 4.

We develop the following variants of the RASA algorithm:

- RASA-L, which adapts only the row subspace.
- RASA-R, which adapts only the column subspace.
- RASA-LR, which adapts both the row and column subspaces.

It should be noted that when  $\mathcal{M}$  is isomorphic to  $\mathbb{R}^n$ , the adaptive weight vector  $\mathbf{r}_t$  reduces to a scalar. Hence, in this setting, RASA-LR is equivalent to RASA-L (up to a scalar multiple of the adaptive weight vector  $\mathbf{l}_t$ ).

## 4 Convergence rate analysis

For the purpose of analyzing the convergence rate for the proposed Algorithm 1, we view our proposed update, step 8 in Algorithm 1, as

$$x_{t+1} = R_{x_t}(-\alpha_t\mathcal{P}_{x_t}(\hat{\mathbf{V}}_t^{-1/2}\mathbf{g}_t(x_t))), \quad (11)$$

where  $t$  represents the iteration number,  $\hat{\mathbf{V}}_t = \text{Diag}(\hat{\mathbf{v}}_t)$ , and  $\hat{\mathbf{v}}_t$  is defined as

$$\hat{\mathbf{v}}_t = \hat{\mathbf{r}}_t^{1/2} \otimes \hat{\mathbf{l}}_t^{1/2}, \quad (12)$$

where the symbol ‘ $\otimes$ ’ represents the Kronecker product and  $\mathbf{g}_t(x)$  denotes the vectorized representation of  $\text{grad}f_t(x)$ . Furthermore,  $\mathbf{g}(x)$  denotes the vectorized representation of  $\text{grad}f(x)$ . Hence,  $\hat{\mathbf{v}}_t$ ,  $\mathbf{g}_1(x)$ ,  $\mathbf{g}_t(x)$ , and  $\mathbf{g}(x)$  are  $nr$  dimensional vectors in our analysis. We first summarize essential assumptions and a lemma before discussing our main results.

## 4.1 Definitions and assumptions

For simplicity, the analysis hereinafter assumes the standard Riemannian metric as  $g(\xi, \eta)_x := \langle \xi, \eta \rangle_2$  (Euclidean inner product) and the standard Riemannian norm as  $\|\xi\|_x := \|\xi\|_2$  (Euclidean norm), where  $\xi, \eta \in T_x\mathcal{M}$ .

**Definition 4.1. Upper-Hessian bounded** (Absil et al., 2008). *The function  $f$  is said to be upper-Hessian bounded in  $\mathcal{U} \subset \mathcal{M}$  with respect to retraction  $R$  if there exists a constant  $L > 0$  such that  $\frac{d^2 f(R_x(t\eta))}{dt^2} \leq L$ , for all  $x \in \mathcal{U}$  and  $\eta \in T_x\mathcal{M}$  with  $\|\eta\|_x = 1$ , and all  $t$  such that  $R_x(\tau\eta) \in \mathcal{U}$  for all  $\tau \in [0, t]$ .*

The above class of functions in the Riemannian setting corresponds to the set of continuous functions with Lipschitz continuous gradients in the Euclidean space.

We now state our assumptions on problem (4).

**Assumption 1.** *For problem (4), we assume the following:*

(A1) *The function  $f$  is continuously differentiable and is lower bounded, i.e.,  $f(x^*) > -\infty$  where  $x^*$  is an optimal solution of (4).*

(A2) *The function  $f$  has  $H$ -bounded Riemannian stochastic gradient, i.e.,  $\|\text{grad} f_i(x)\|_F \leq H$  or equivalently  $\|\mathbf{g}_i(x)\|_2 \leq H$ .*

(A3) *The function  $f$  is upper-Hessian bounded.*

Existing works (Zhou et al., 2018; Chen et al., 2019), which focus on the convergence of (Euclidean) ADAM (Kingma & Ba, 2015), use a Euclidean variant of A2. Furthermore, A2 holds when the manifold is compact like the Grassmann manifold (Absil et al., 2008), or through slight modification of the objective function and the algorithm (Kasai et al., 2018b).

Finally, we define Retraction  $L$ -smooth functions via the following lemma.

**Lemma 4.2. Retraction  $L$ -smooth** (Huang et al., 2015; Kasai et al., 2018b). *Suppose Assumption 1 holds. Then, for all  $x, y \in \mathcal{M}$  and constant  $L > 0$  in Definition 4.1, we have*

$$f(z) \leq f(x) + \langle \text{grad} f(x), \xi \rangle_2 + \frac{1}{2}L\|\xi\|_2^2, \quad (13)$$

where  $\xi \in T_x\mathcal{M}$  and  $R_x(\xi) = z$ . In particular, such a function  $f$  is called retraction  $L$ -smooth with respect to  $R$ .

The proof of Lemma 4.2 is provided in (Kasai et al., 2018b, Lemma 3.5). Refer (Boumal et al., 2018) for other means to ensure Retraction  $L$ -smoothness of a function.

## 4.2 Convergence analysis of Algorithm 1

Our proof structure extends existing convergence analysis of ADAM-type algorithms in the Euclidean space (Zhou et al., 2018; Chen et al., 2019) into the Riemannian setting. However, such an extension is non-trivial and key challenges include

- the update formula based on  $\hat{\mathbf{r}}_t$  and  $\hat{\mathbf{I}}_t$  in Algorithm 1 requires the upper bound of  $\hat{\mathbf{v}}_t$  defined in (12).
- projection onto the tangent space: the Riemannian gradient adaptively weighted by  $\hat{\mathbf{r}}_t$  and  $\hat{\mathbf{I}}_t$  needs to be projected back onto a tangent space. Our analysis needs to additionally take care of this.

To this end, we first provide a lemma for the upper bounds of the full Riemannian gradient as well as the elements of the vector  $\hat{\mathbf{v}}_t$ , where  $\hat{\mathbf{l}}_t$  and  $\hat{\mathbf{r}}_t$  are defined in steps 4 – 7 of Algorithm 1.

**Lemma 4.3.** *Let  $\hat{\mathbf{v}}_t = \hat{\mathbf{r}}_t^{1/2} \otimes \hat{\mathbf{l}}_t^{1/2}$ , where  $\hat{\mathbf{l}}_t$  and  $\hat{\mathbf{r}}_t$  are defined in steps 4 – 7 in Algorithm 1. Then, under Assumption 1, we have the following results*

- $\|\text{grad}f(x)\|_F \leq H$ , and
- the  $j$ -th element of  $\hat{\mathbf{v}}_t$  satisfies  $(\hat{\mathbf{v}}_t)_j \leq H^2$ .

We now present our main result in Theorem 4.4.

**Theorem 4.4.** *Let  $\{x_t\}$  and  $\{\hat{\mathbf{v}}_t\}$  be the sequences obtained from Algorithm 1, where  $\hat{\mathbf{v}}_t = \hat{\mathbf{r}}_t^{1/2} \otimes \hat{\mathbf{l}}_t^{1/2}$ . Then, under Assumption 1, we have the following results for Algorithm 1*

$$\begin{aligned} & \mathbb{E} \left[ \sum_{t=2}^T \alpha_{t-1} \left\langle \mathbf{g}(x_t), \frac{\mathbf{g}(x_t)}{\sqrt{\hat{\mathbf{v}}_{t-1}}} \right\rangle_2 \right] \\ & \leq \mathbb{E} \left[ \frac{L}{2} \sum_{t=1}^T \left\| \frac{\alpha_t \mathbf{g}_t(x_t)}{\sqrt{\hat{\mathbf{v}}_t}} \right\|_2^2 + H^2 \sum_{t=2}^T \left\| \frac{\alpha_t}{\sqrt{\hat{\mathbf{v}}_t}} - \frac{\alpha_{t-1}}{\sqrt{\hat{\mathbf{v}}_{t-1}}} \right\|_1 \right] \\ & \quad + C, \end{aligned} \tag{14}$$

where  $C$  is a constant term independent of  $T$ .

**Proof sketch:** We first derive a Retraction  $L$ -smooth inequality from Lemma 4.2 with respect to the adaptive gradient  $\mathcal{P}_{x_t}(\hat{\mathbf{V}}_t^{-1/2} \mathbf{g}_t(x_t))$ . Exploiting the symmetric property of  $\mathcal{P}_{x_t}$ , we obtain the upper bound of  $-\langle \mathbf{g}(x_t), \alpha_t \mathcal{P}_{x_t}(\hat{\mathbf{V}}_t^{-1/2} \mathbf{g}_t(x_t)) \rangle_2$ . Here, to remove the dependency of  $\hat{\mathbf{V}}_t$  on  $\mathbf{g}_t(x_t)$ ,  $\hat{\mathbf{V}}_{t-1}^{-1/2} \mathbf{g}_t(x_t)$  is evaluated instead of  $\hat{\mathbf{V}}_t^{-1/2} \mathbf{g}_t(x_t)$ . Then, taking the expectation and telescoping the inequality, we obtain the desired result. The complete proof is in Section A.

**Remark 2:** The first term of (14) represents the weighted term of the sum of squared step length, and appears in the standard RSGD (Bonnabel, 2013). From this point of view, the advantage of the adaptive gradient algorithms can be seen that they reduce the effect of the term  $\mathbb{E}[\sum_{t=1}^T \|\alpha_t \mathbf{g}_t(x_t) / \sqrt{\hat{\mathbf{v}}_t}\|_2^2]$  compared with the standard RSGD algorithm.

**Remark 3:** Theorem 4.4 reproduces the results of (Chen et al., 2019, Theorem 3.1) when  $\mathcal{M}$  is defined as the Euclidean space.

In Corollary 4.5, we derive a convergence rate of Algorithm 1.

**Corollary 4.5** (Convergence rate of Algorithm 1). *Let  $\{x_t\}$  and  $\{\hat{\mathbf{v}}_t\}$  be the sequences obtained from Algorithm 1, where  $\hat{\mathbf{v}}_t = \hat{\mathbf{r}}_t^{1/2} \otimes \hat{\mathbf{l}}_t^{1/2}$ . Let  $\alpha_t = 1/\sqrt{t}$  and  $\min_{j \in [d]} \sqrt{(\hat{\mathbf{v}}_1)_j}$  is lower-bounded by a constant  $c > 0$ , where  $d$  is the dimension of the manifold  $\mathcal{M}$ . Then, under Assumption 1, the output of  $x_t$  of Algorithm 1 satisfies*

$$\min_{t \in [2, \dots, T]} \mathbb{E} \|\text{grad}f(x_t)\|_F^2 \leq \frac{1}{\sqrt{T-1}} (Q_1 + Q_2 \log(T)), \tag{15}$$

where  $Q_2 = LH^3/2c^2$  and

$$Q_1 = Q_2 + \frac{2dH^3}{c} + H\mathbb{E}[f(x_1) - f(x^*)]. \tag{16}$$



## 5 Related works

The asymptotic convergence of stochastic gradient descent on Riemannian manifolds (RSGD) was proved by Bonnabel (2013). Among the first works to adapt stochastic gradients on Riemannian matrix manifolds is the cRMSPProp algorithm (Roy et al., 2018). They effectively perceive adaptive weights as vectors. More concretely, if elements in  $\mathcal{M}$  have matrix representation of size  $n \times r$ , then cRMSPProp computes an adaptive weight matrix  $\mathbf{A} \in \mathbb{R}^{n \times r}$  and adapts the gradient matrix  $\mathbf{H} \in \mathbb{R}^{n \times r}$  as  $\mathbf{A} \circ \mathbf{H}$ . It can be observed that this interpretation of adaptive weights ignores the matrix structure of  $\mathbf{A}$ ,  $\mathbf{H}$ , and in general  $\mathcal{M}$ , and process adaptive weights similar to the Euclidean algorithms discussed in Section 2. Roy et al. (2018) also constrain the adaptive weight matrix  $\mathbf{A}$  to lie on the tangent plane, thereby requiring computationally expensive vector transport operations in each iteration. It should also be noted that Roy et al. (2018) do not provide convergence analysis for cRMSPProp.

Another direction of work by Cho & Lee (2017); Bécigneul & Ganea (2019) derive the ADAM algorithm (Kingma & Ba, 2015) on matrix manifolds. In particular, they employ a momentum term along with the Riemannian gradient to compute the search direction. However, the adaptive weight vector in the ADAM algorithm is now substituted with a scalar weight, which effectively adapts the step size rather than the search direction. While Cho & Lee (2017) do not discuss convergence analysis, Bécigneul & Ganea (2019) provide convergence guarantees limited to geodesically convex functions (Zhang & Sra, 2016). It should be noted that both require vector transport operations in each iteration due to the momentum term.

Our approach, on the other hand, preserves the underlying matrix structure of the manifold and compute adaptive weight matrices corresponding to row and column subspaces of the Riemannian gradient. We do not enforce any constraint on the adaptive weight matrices and avoid parallel transport altogether. Our algorithm can be easily be generalized to product of manifolds.

Existing works have also explored other directions of improvement to RSGD in specific settings, similar to the Euclidean counterpart. These include variance reduction (Zhang et al., 2016; Sato et al., 2019), averaged RSGD (Tripuraneni et al., 2018), recursive gradients (Kasai et al., 2018b), incorporating second-order information (Kasai et al., 2018a; Kasai & Mishra, 2018), among others.

In the Euclidean setting, structure-aware preconditioners for (unconstrained) stochastic optimization over matrices or tensors has been discussed in (Martens & Grosse, 2015; Gupta et al., 2018).

## 6 Experiments

In this section, we compare our proposed adaptive algorithm, RASA, and its variants with the following baseline Riemannian stochastic algorithms.

- RSGD (Bonnabel, 2013) is the vanilla Riemannian stochastic gradient algorithm.
- cRMSPProp proposed by Roy et al. (2018).
- cRMSPProp-M: a variant of cRMSPProp, which uses Riemannian gradients for adaptive weights computations instead of the Euclidean gradients.
- Radagrads proposed by Bécigneul & Ganea (2019) considers scalar adaptive weight. Hence, it adapts the step size instead of the gradient.

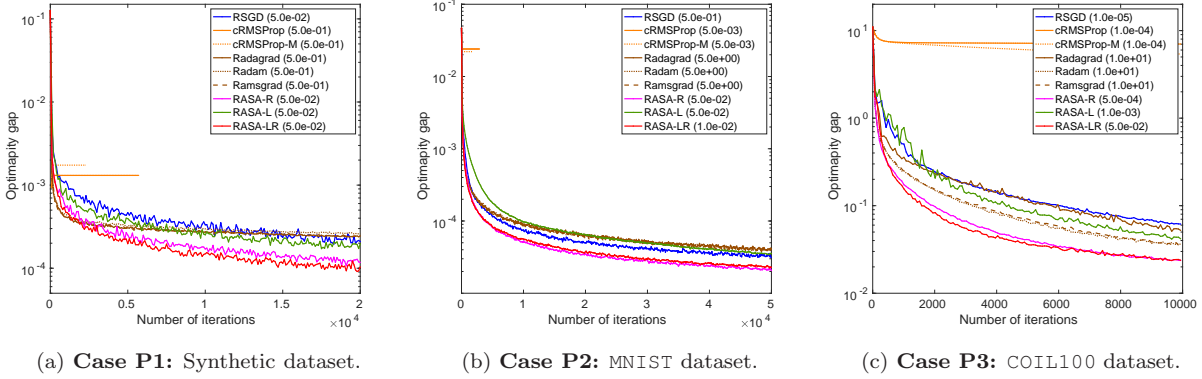


Figure 1: Performance on the PCA datasets (numbers in the parentheses within legends show best-tuned  $\alpha_0$ ).

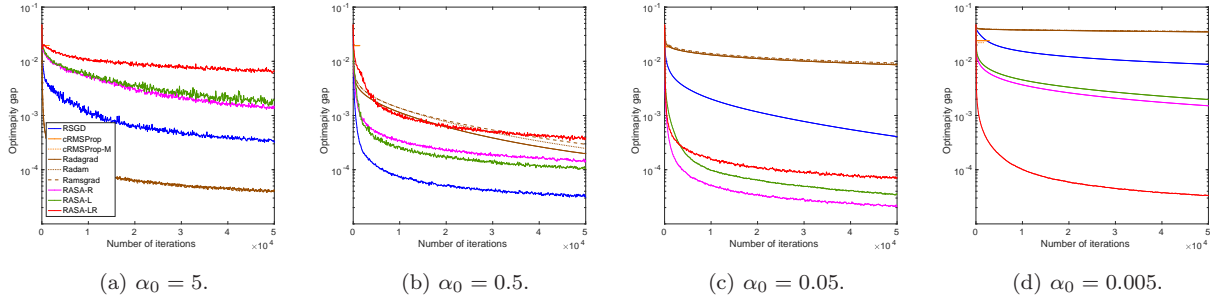


Figure 2: Performance on the MNIST dataset across different values of the initial step size  $\alpha_0$  (**Case P2**).

- Radam and Ramsgrad by Bécigneul & Ganea (2019): include momentum terms similar to ADAM and AMSGrad. Additionally, like Radagradd, they adapt only the step size.
- RASA-L, RASA-R, and RASA-LR: our proposed variants that either adapt the row (left) subspace, column (right) subspace, or both.

All the considered algorithms are implemented in the Matlab toolbox Manopt (Boumal et al., 2014). The codes are available at <https://github.com/hiroyuki-kasai/RSOpt>. For deep learning applications, RASA can be implemented in Python libraries like McTorch (Meghwanshi et al., 2018) and geomstats (Miolane et al., 2018).

The algorithms are initialized from the same initialization point and are stopped when the iteration count reaches a predefined value. We fix the batchsize to 10 (except in the larger MovieLens datasets, where it is set to 100). The step size sequence  $\{\alpha_t\}$  is generated as  $\alpha_t = \alpha_0/\sqrt{t}$  (Chen et al., 2019; Reddi et al., 2018), where  $t$  is the iteration count. We experiment with different values for the initial step size  $\alpha_0$ . The  $\beta$  value for adaptive algorithms (all except RSGD) is fixed to 0.99. The momentum-related  $\beta$  term (used only in Radam and Ramsgrad) is set to 0.9 (Bécigneul & Ganea, 2019).

We address the principal component analysis (PCA) and the independent component analysis

(ICA) problems on the Stiefel manifold  $\text{St}(r, n)$ : the set of orthogonal  $r$ -frames in  $\mathbb{R}^n$  for some  $r \leq n$  (Absil et al., 2008). The elements of  $\text{St}(r, n)$  are represented as matrices of size  $n \times r$ . We also consider the low-rank matrix completion (MC) problem on the Grassmann manifold  $\text{Gr}(r, n)$ , which is the set of  $r$ -dimensional subspaces in  $\mathbb{R}^n$  and is a Riemannian quotient manifold of the Stiefel manifold (Absil et al., 2008).

Apart from the results discussed in this section, Section B contains additional results including performance of the algorithms across different values of  $\alpha_0$ , time dependency plots, and decreasing moving average scheme for RASA.

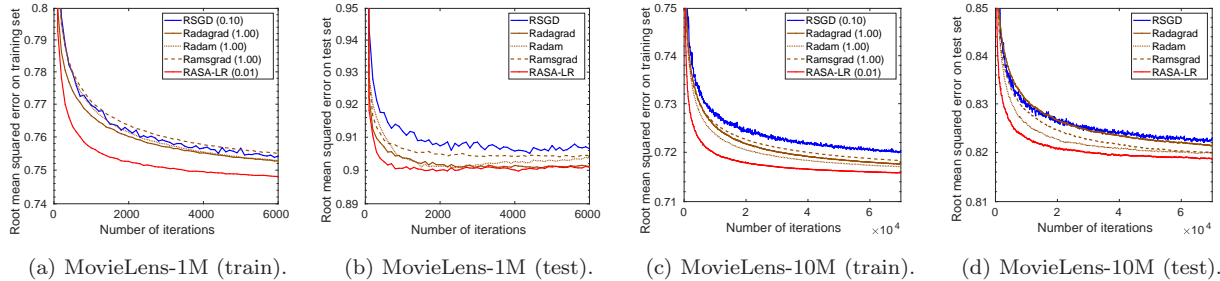


Figure 3: Performance on the MovieLens datasets (numbers in the parentheses within legends show best-tuned  $\alpha_0$ ). Our proposed algorithm RASA-LR performs competitively and shows faster convergence.

## 6.1 Principal components analysis

Given a set of data points  $\{\mathbf{z}_1, \dots, \mathbf{z}_N\} \in \mathbb{R}^n$ , the PCA problem amounts to learning an orthogonal projector  $\mathbf{U} \in \text{St}(r, n)$  that minimizes the sum of squared residual errors between projected data points and the original data points. It is formulated as  $\min_{\mathbf{U} \in \text{St}(r, n)} \frac{1}{N} \sum_{i=1}^N \|\mathbf{z}_i - \mathbf{U}\mathbf{U}^\top \mathbf{z}_i\|_2^2$ . This problem is equivalent to  $\min_{\mathbf{U} \in \text{St}(r, n)} -\frac{1}{N} \sum_{i=1}^N \mathbf{z}_i^\top \mathbf{U}\mathbf{U}^\top \mathbf{z}_i$ .

We first evaluate the algorithms on a synthetic dataset of size  $(N, n, r) = (10^4, 10^2, 10)$  (**Case P1**). The initial step size  $\alpha_0$  is selected from the set  $\{0.5, 0.1, \dots, 5 \times 10^{-3}, 10^{-3}\}$ . Figure 1 (a) shows *optimality gap* with best-tuned step sizes of each algorithm. The minimum loss for the optimality gap computation is obtained by the Matlab command `pca`. We observe that our algorithms RASA-LR and RASA-R obtain the best solution. On the other hand, cRMSProp and its modified variant cRMSProp-M converge poorly. Radagrad and its momentum based variants (Ramsgrad and Radam) initially proceed well but finally converge to a solution slightly worse than RSGD.

We additionally evaluate RASA on the MNIST (**Case P2**) and COIL100 (**Case P3**) datasets in the same setting as described in **Case P1**. MNIST contains handwritten digits data of 0 – 9 (LeCun et al.) and has 60 000 images for training and 10 000 images for testing with images of size  $28 \times 28$ . For MNIST,  $(N, n, r) = (10^4, 784, 10)$  and the  $\alpha_0$  is selected from the set  $\{10, 5, \dots, 10^{-2}, 5 \times 10^{-3}\}$ . COIL100 contains normalized 7 200 color camera images of the 100 objects taken from different angles (Nene et al., 1996a). We resize them into  $32 \times 32$  pixels. For COIL100,  $(N, n, r) = (7200, 1024, 100)$  and the  $\alpha_0$  is selected from the set  $\{50, 10, \dots, 10^{-5}, 5 \times 10^{-6}\}$ . From Figures 1 (b)–(c), we observe that RASA-LR and RASA-R perform better than other baselines on both MNIST

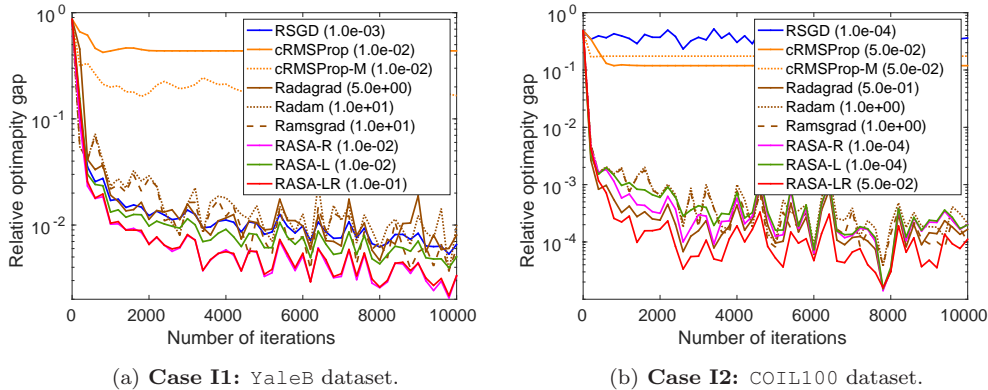


Figure 4: Performance on the ICA problem (numbers in the parentheses within legends show best-tuned  $\alpha_0$ ).

and COIL100 datasets. This shows the benefit of adapting the row and column subspaces over individual entries on Riemannian manifolds.

In order to observe the influence of the choice of  $\alpha_0$  on the algorithms, we plot the results of all the algorithms on the MNIST dataset for  $\alpha_0 = \{5, 0.5, 0.05, 0.005\}$  in Figure 2. It can be seen that the proposed algorithms are more robust to changes in  $\alpha_0$  than other adaptive algorithms. As discussed before, RASA-LR and RASA-R obtain the best results on this dataset.

## 6.2 Joint diagonalization in ICA

The ICA or the blind source separation problem refers to separating a signal into components so that the components are as independent as possible (Hyvärinen & Oja, 2000). A particular preprocessing step is the whitening step that is proposed through joint diagonalization on the Stiefel manifold (Theis et al., 2009). To that end, the optimization problem of interest is  $\min_{\mathbf{U} \in \mathbb{R}^{n \times r}} -\frac{1}{N} \sum_{i=1}^N \|\text{diag}(\mathbf{U}^\top \mathbf{C}_i \mathbf{U})\|_F^2$ , where  $\|\text{diag}(\mathbf{A})\|_F^2$  defines the sum of the squared diagonal elements of  $\mathbf{A}$ . The symmetric matrices  $\mathbf{C}_i$ s are of size  $n \times n$  and can be cumulant matrices or time-lagged covariance matrices of  $N$  different signal samples (Theis et al., 2009).

We use the `YaleB` (Georghiadis et al., 2001) dataset (**Case I1**), which contains human subjects images under different poses and illumination conditions. The image size of the original images is  $168 \times 192$ . From this dataset, we create a region covariance matrix (RCM) descriptors (Porikli & Tuzel, 2006; Tuzel et al., 2006; Pang et al., 2008) for 2015 images, and the resultant RCMs are of size  $40 \times 40$ . The initial step size  $\alpha_0$  is selected from  $\{10, 5, \dots, 5 \times 10^{-4}, 10^{-4}\}$  and we set  $r = 30$ . For `YaleB`,  $(N, n, r) = (2015, 40, 30)$ . We also use the `COIL100` dataset (**Case I2**). The RCM descriptors of size  $7 \times 7$  from 7200 images are created. The initial step size  $\alpha_0$  is selected from  $\{10, 5, \dots, 5 \times 10^{-4}, 10^{-4}\}$  and we set  $r = 7$ . Thus,  $(N, n, r) = (7200, 7, 7)$ . We show plots for *relative* optimality gap (ratio of optimality gap to the optimal objective value) for all the algorithms in Figure 4. The optimal solution value for optimality gap computation is obtained from the algorithm proposed by Theis et al. (2009). We observe that adapting both left and right subspaces (RASA-LR) leads to the best results on both the datasets.

### 6.3 Low-rank matrix completion

The low-rank matrix completion problem amounts to completing an incomplete matrix  $\mathbf{Z}$ , say of size  $n \times N$ , from a small number of observed entries by assuming a low-rank model for  $\mathbf{Z}$ . If  $\Omega$  is the set of the indices for which we know the entries in  $\mathbf{Z}$ , then the rank- $r$  matrix completion problem amounts to finding matrices  $\mathbf{U} \in \mathbb{R}^{n \times r}$  and  $\mathbf{A} \in \mathbb{R}^{r \times N}$  that minimizes the error  $\|(\mathbf{U}\mathbf{A})_{\Omega} - \mathbf{Z}_{\Omega}\|_F^2$ . Partitioning  $\mathbf{Z} = [\mathbf{z}_1, \mathbf{z}_2, \dots, \mathbf{z}_N]$  and exploiting the least squares structure (Boumal & Absil, 2015b), the problem is equivalent to  $\min_{\mathbf{U} \in \text{Gr}(r, n)} \frac{1}{N} \sum_{i=1}^N \|(\mathbf{U}\mathbf{a}_i)_{\Omega_i} - \mathbf{z}_{i\Omega_i}\|_2^2$ , where  $\mathbf{z}_i \in \mathbb{R}^n$  and  $\Omega_i$  is the set of observed indices for  $i$ -th column.

We show the results on the MovieLens datasets (Harper & Konstan, 2015) which consist of ratings of movies given by different users. The MovieLens-10M dataset consists of 10 000 054 ratings by 71 567 users for 10 677 movies. The MovieLens-1M dataset consists of 1 000 209 ratings by 6 040 users for 3 900 movies. We randomly split the data into 80/20 train/test partitions. We run different algorithms for rank  $r = 10$  and regularization parameter 0.01 as suggested by Boumal & Absil (2015b). Figures 3 (a)-(d) show that our algorithm RASA-LR achieves faster convergence during the training phase and the best generalization performance on the test set. cRMSPProp and cRMSPProp-M did not run successfully on MovieLens datasets for different choices of  $\alpha_0$ .

### 6.4 RASA-vec: a vectorized variant of RASA

We end this section noting that the effective dimension of our adaptive weights (vectors  $\hat{\mathbf{l}}_t$  and  $\hat{\mathbf{r}}_t$ ) in Algorithm 1 is  $n+r$ , which is less than the ambient dimension  $nr$  of the Riemannian gradient  $\mathbf{G}_t$ . In Euclidean algorithms such as ADAM, AMSGrad (Reddi et al., 2018), AdaGrad, or RMSProp, the effective dimension of the adaptive weights is same as the Euclidean gradient. To observe the effect of the proposed reduction in dimension of adaptive weights in the Riemannian setting, we develop a variant of RASA, called RASA-vec, which directly updates all the entries of the Riemannian gradient. That is, for RASA-vec, the Riemannian gradient is adapted as

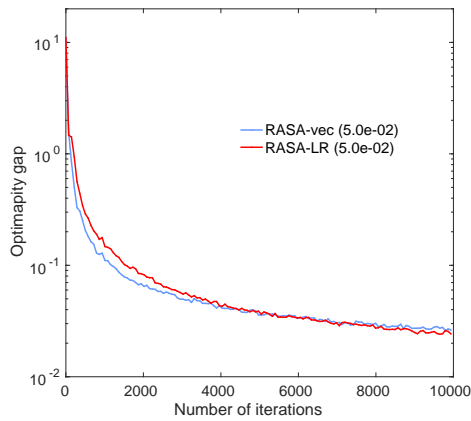
$$\text{vec}(\tilde{\mathbf{G}}_t) = \hat{\mathbf{V}}_t^{-1/2} \text{vec}(\mathbf{G}_t),$$

where the adaptive weights matrix is  $\hat{\mathbf{V}}_t = \text{Diag}(\hat{\mathbf{v}}_t)$ ,  $\hat{\mathbf{v}}_t = \max(\mathbf{v}_t, \hat{\mathbf{v}}_{t-1})$ , and  $\mathbf{v}_t = \beta \mathbf{v}_{t-1} + (1 - \beta) \text{vec}(\mathbf{G}_t) \circ \text{vec}(\mathbf{G}_t)$ . Here, the symbol ‘ $\circ$ ’ denotes the entry-wise product (Hadamard product) of vectors. The update strategy of RASA-vec remains same as that of RASA in (11), i.e.,  $x_{t+1} = R_x(-\alpha_t \mathcal{P}_{x_t}(\tilde{\mathbf{G}}_t))$ . The convergence guarantees of RASA-vec also follow naturally from Section 4.

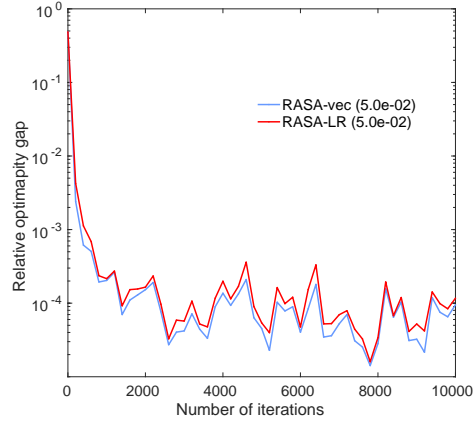
Figure 5 compares the performance of the RASA-LR with RASA-vec on the three problems discussed earlier. The results illustrate the benefits of the proposed modeling approach that we RASA-LR achieves similar performance to RASA-vec even though it stores  $n+r$  adaptive weights instead of  $nr$  weights.

## 7 Discussion and conclusion

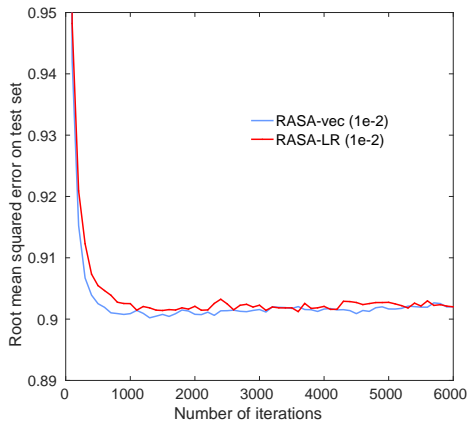
We observe that the proposed modeling of adaptive weights on the row and column subspaces obtains better empirical performance than existing baselines (Roy et al., 2018; Cho & Lee, 2017; Bécigneul & Ganea, 2019). In particular, we do not observe additional benefit of the adaptive momentum methods (Radam and Ramsgrad) in the Riemannian setting when the adaptive updates exploit the geometry better.



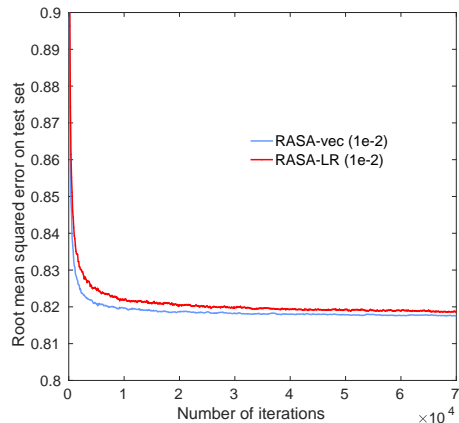
(a) PCA on COIL100 dataset.



(b) ICA COIL100 dataset.



(c) MovieLens-1M (test).



(d) MovieLens-10M (test).

Figure 5: Similar performance of RASA-vec and RASA-LR on different datasets (numbers in the parentheses within legends show best-tuned  $\alpha_0$ ).

Overall, we presented a principled approach for modeling adaptive weights for Riemannian stochastic gradient on matrix manifolds. We developed computationally efficient algorithms and discussed the convergence analysis. Our experiments validate the benefits of the proposed algorithms on different applications.

## Acknowledgements

H. Kasai was partially supported by JSPS KAKENHI Grant Numbers JP16K00031 and JP17H01732.

## References

- Absil, P.-A., Mahony, R., and Sepulchre, R. *Optimization Algorithms on Matrix Manifolds*. Princeton University Press, 2008.
- Bécigneul, B. and Ganea, O.-E. Riemannian adaptive optimization methods. In *ICLR*, 2019.
- Bonnabel, S. Stochastic gradient descent on Riemannian manifolds. *IEEE Trans. Autom. Control*, 58(9):2217–2229, 2013.
- Bottou, L., Curtis, F. E., and Nocedal, J. Optimization methods for large-scale machine learning. *SIAM Rev.*, 60(2):223–311, 2018.
- Boumal, N. and Absil, P.-A. Low-rank matrix completion via preconditioned optimization on the Grassmann manifold. *Linear Algebra and its Applications*, 475:200–239, 2015a.
- Boumal, N. and Absil, P.-A. Low-rank matrix completion via preconditioned optimization on the Grassmann manifold. *Linear Algebra Its Appl.*, 475:200–239, 2015b.
- Boumal, N., Mishra, B., Absil, P.-A., and Sepulchre, R. Manopt, a Matlab toolbox for optimization on manifolds. *J. Mach. Learn. Res.*, 15(1):1455–1459, 2014.
- Boumal, N., Absil, P.-A., and Cartis, C. Global rates of convergence for nonconvex optimization on manifolds. *IMA J. Numer. Anal.*, 2018.
- Chen, X., Liu, S., Sun, R., and Hong, M. On the convergence of a class of Adam-type algorithms for non-convex optimization. In *ICLR*, 2019.
- Cho, M. and Lee, J. Riemannian approach to batch normalization. In *NIPS*, 2017.
- Duchi, J., Hazan, E., and Singer, Y. Adaptive subgradient methods for online learning and stochastic optimization. *J. Mach. Learn. Res.*, 12:2121–2159, 2011.
- Ganea, O.-E., Bécigneul, B., and Hofmann, T. Hyperbolic entailment cones for learning hierarchical embeddings. In *ICML*, 2018.
- Georgiades, A., Belhumeur, P., and Kriegman, D. From few to many: Illumination cone models for face recognition under variable lighting and pose. *IEEE Trans. Pattern Anal. Mach. Intelligence*, 23(6):643–660, 2001.
- Goldberg, K., Roeder, T., Gupta, D., and Perkins, C. Eigentaste: a constant time collaborative filtering algorithm. *Inform. Retrieval*, 4(2):133–151, 2001.
- Gupta, V., Koren, T., and Singer, Y. Shampoo: Preconditioned stochastic tensor optimization. In *ICML*, 2018.
- Harandi, M., Salzmann, M., and Hartley, R. Joint dimensionality reduction and metric learning: A geometric take. In *ICML*, 2017a.
- Harandi, M., Salzmann, M., and Richard, H. Dimensionality reduction on spd manifolds: The emergence of geometry-aware methods. *IEEE Trans. Pattern Anal. Mach. Intell.*, 2017b.

- Harper, F. M. and Konstan, J. A. The MovieLens datasets: history and context. *ACM Trans. Interact. Intell. Syst.*, 5(4):19:1–19:19, 2015.
- Huang, W., Gallivan, K. A., and Absil, P.-A. A Broyden class of quasi-Newton methods for Riemannian optimization. *SIAM J. Optim.*, 25(3):1660–1685, 2015.
- Hyvärinen, A. and Oja, E. Independent component analysis: algorithms and applications. *Neural Netw.*, 13(4-5):411–430, 2000.
- Jawanpuria, P. and Mishra, B. A unified framework for structured low-rank matrix learning. In *ICML*, 2018.
- Jawanpuria, P., Balgovind, A., Kunchukuttan, A., and Mishra, B. Learning multilingual word embeddings in latent metric space: A geometric approach. *Trans. Assoc. Comput. Linguist.*, 7: 07–120, 2019.
- Kasai, H. and Mishra, B. Low-rank tensor completion: a Riemannian manifold preconditioning approach. In *ICML*, 2016.
- Kasai, H. and Mishra, B. Inexact trust-region algorithms on Riemannian manifolds. In *NeurIPS*, 2018.
- Kasai, H., Sato, H., and Mishra, B. Riemannian stochastic quasi-Newton algorithm with variance reduction and its convergence analysis. In *AISTATS*, 2018a.
- Kasai, H., Sato, H., and Mishra, B. Riemannian stochastic recursive gradient algorithm. In *ICML*, 2018b.
- Kingma, D. P. and Ba, J. Adam: A method for stochastic optimization. In *ICLR*, 2015.
- LeCun, Y., Cortes, C., and Burges, C. J. The MNIST database. <http://yann.lecun.com/exdb/mnist/>.
- Lee, J. M. *Introduction to smooth manifolds*, volume 218 of *Graduate Texts in Mathematics*. Springer-Verlag, New York, second edition, 2003.
- Martens, J. and Grosse, R. Optimizing neural networks with Kronecker-factored approximate curvature. In *ICML*, 2015.
- McMahan, H. B. and Streeter, M. Adaptive bound optimization for online convex optimization. In *COLT*. 2010.
- Meghwanshi, M., Jawanpuria, P., Kunchukuttan, A., Kasai, H., and Mishra, B. Mtorch, a manifold optimization library for deep learning. Technical report, arXiv preprint arXiv:1810.01811, 2018.
- Miolane, N., Mathe, J., Donnat, C., Jorda, M., and Pennec, X. geomstats: a python package for riemannian geometry in machine learning. Technical report, arXiv preprint arXiv:1805.08308, 2018.
- Mishra, B. and Sepulchre, R. R3MC: A Riemannian three-factor algorithm for low-rank matrix completion. In *IEEE CDC*, 2014.



- Mishra, B., Kasai, H., Jawanpuria, P., and Saroop, A. A Riemannian gossip approach to subspace learning on grassmann manifold. *Mach. Learn.*, 2019.
- Nene, S. A., Nayar, S. K., and Murase, H. Columbia object image library (COIL-100). Technical report, CUCS-006-96, 1996a.
- Nene, S. A., Nayar, S. K., and Murase, H. Columbia university image library (COIL-20). Technical Report CUCS-005-96, 1996b.
- Nickel, M. and Kiela, D. Poincaré embeddings for learning hierarchical representations. In *NIPS*, 2017.
- Nickel, M. and Kiela, D. Learning continuous hierarchies in the Lorentz model of hyperbolic geometry. In *ICML*, 2018.
- Nimishakavi, M., Jawanpuria, P., and Mishra, B. A dual framework for low-rank tensor completion. In *NeurIPS*, 2018.
- Pang, Y., Yuan, Y., and Li, X. Gabor-based region covariance matrices for face recognition. *IEEE Trans. Circuits Syst. Video Technol.*, 18(7):989–993, 2008.
- Pennington, J., Socher, R., and Manning, C. Glove: Global vectors for word representation. In *EMNLP*, 2014.
- Porikli, F. and Tuzel, O. Fast construction of covariance matrices for arbitrary size image windows. In *ICIP*, 2006.
- Reddi, S. J., Kale, S., and Kumar, S. On the convergence of Adam and beyond. In *ICLR*, 2018.
- Roy, S. K., Mhammedi, Z., and Harandi, M. Geometry aware constrained optimization techniques for deep learning. In *CVPR*, 2018.
- Sato, H., Kasai, H., and Mishra, B. Riemannian stochastic variance reduced gradient algorithm with retraction and vector transport. *SIAM J. Optim.*, 29(2):1444–1472, 2019.
- Shah, V., Kyrillidis, A., and Sanghavi, S. Minimum norm solutions do not always generalize well for over-parameterized problems. Technical report, arXiv preprint arXiv:1811.07055, 2018.
- Theis, F. J., Cason, T. P., and Absil, P.-A. Soft dimension reduction for ICA by joint diagonalization on the Stiefel manifold. In *ICA*, 2009.
- Tieleman, T. and Hinton, G. RMSProp: Divide the gradient by a running average of its recent magnitude. COURSERA: Neural Networks for Machine Learning, 2012.
- Tripuraneni, N., Flammarion, N., Bach, F., and Jordan, M. I. Averaging stochastic gradient descent on Riemannian manifolds. In *COLT*, 2018.
- Tuzel, O., Porikli, F., and Meer, P. Region covariance: a fast descriptor for detection and classification. In *ECCV*, 2006.
- Vandereycken, B. Low-rank matrix completion by Riemannian optimization. *SIAM J. Optim.*, 23(2):1214–1236, 2013.

- Ward, R., Wu, X., and Bottou, L. Adagrad stepsizes: Sharp convergence over nonconvex landscapes, from any initialization. *arXiv preprint arXiv:1806.01811*, 2018.
- Wilson, A. C., Roelofs, R., Stern, M., Srebro, N., and Recht, B. The marginal value of adaptive gradient methods in machine learning. In *NIPS*. 2017.
- Zaheer, M., Reddi, S., Sachan, D., Kale, S., and Kumar, S. Adaptive methods for nonconvex optimization. In *NeurIPS*. 2018.
- Zeiler, M. D. ADADELTA: An adaptive learning rate method. Technical report, arXiv preprint arXiv:1212.5701, 2012.
- Zhang, H. and Sra, S. First-order methods for geodesically convex optimization. In *COLT*, 2016.
- Zhang, H., Reddi, S. J., and Sra, S. Riemannian SVRG: fast stochastic optimization on Riemannian manifolds. In *NIPS*, 2016.
- Zhou, D., Tang, Y., Yang, Z., Cao, Y., and Gu, Q. On the convergence of adaptive gradient methods for nonconvex optimization. Technical report, arXiv preprint arXiv:1808.05671, 2018.

## A Proofs

This section provides complete proofs of the lemmas and the convergence analysis.

### A.1 Proof of Lemma 4.3

*Proof.* For any  $x$ , we have

$$\|\text{grad}f(x)\|_F = \|\mathbb{E}_i \text{grad}f_i(x)\|_F \leq \mathbb{E}_i \|\text{grad}f_i(x)\|_F \leq H.$$

Next, we derive the upper bound of the  $p$ -th element ( $p \in [r]$ ) of  $\mathbf{r}_t$ , i.e.,  $(\mathbf{r}_t)_p$ . Denoting  $(\mathbf{r}_t)_p$  as  $r_{t,p}$  for simplicity, we have  $r_{0,p} = 0$  from the algorithm. Now, we first assume that  $(0 \leq) r_{t,p} \leq H^2$ . Then, addressing  $((\mathbf{G}_t)_{p,q})^2 = g_{p,q}^2 \leq H^2$  due to  $\|\text{grad}f_i(x)\|_F \leq H$ , we have

$$\begin{aligned} r_{t+1,p} &= \beta r_{t,p} + \frac{1-\beta}{n} (\text{diag}(\mathbf{G}_{t+1}^T \mathbf{G}_{t+1}))_p \\ &= \beta r_{t,p} + \frac{1-\beta}{n} \mathbf{G}_{t+1}^T(:,p) \mathbf{G}_{t+1}(:,p) \\ &= \beta r_{t,p} + \frac{1-\beta}{n} \sum_{q=1}^n g_{p,q}^2 \\ &\leq \beta H^2 + \frac{1-\beta}{n} \sum_{q=1}^n H^2 \\ &= \beta H^2 + \frac{1-\beta}{n} n H^2 \\ &\leq H^2. \end{aligned}$$

Consequently, for any  $t \geq 0$ , we have  $r_{t,p} \leq H^2$ . Similarly, having  $l_{0,q} = 0$  for  $q \in [n]$ , and assuming  $(0 \leq) l_{t,q} \leq H^2$ , we have  $l_{t+1,q} \leq H^2$ . Thus, we have  $l_{t,q} \leq H^2$ .

Now, when  $j = n(p-1) + q$ ,  $(\hat{\mathbf{v}}_t)_j = \hat{v}_{t,j} = \hat{r}_{t,p}^{1/2} \times \hat{l}_{t,q}^{1/2}$  due to  $\hat{\mathbf{v}}_t = \hat{\mathbf{r}}_t^{1/2} \otimes \hat{\mathbf{l}}_t^{1/2}$ . Therefore, supposing that  $\hat{r}_{0,p} = \hat{l}_{0,q} = 0$ , and also that  $\hat{r}_{t,p} \leq H^2$  and  $\hat{l}_{t,q} \leq H^2$ , we have

$$\begin{aligned} (\hat{\mathbf{v}}_{t+1})_j &= \hat{v}_{t+1,j} = \hat{r}_{t+1,p}^{1/2} \times \hat{l}_{t+1,q}^{1/2} \\ &= \max(\hat{r}_{t,p}, r_{t+1,p})^{1/2} \times (\hat{l}_{t,q}, l_{t+1,q})^{1/2} \\ &\leq H^2. \end{aligned}$$

Thus, for any  $t \geq 0$ , we have  $(\hat{\mathbf{v}}_t)_j \leq H^2$ .

This completes the proof.  $\square$

### A.2 Proof of Theorem 4.4

This section provides the complete proof of Theorem 4.4.

For this purpose, we first provide an essential lemma for projection matrix as presented below.

**Lemma A.1** (Projection matrix). *Suppose that  $\mathbf{A}\xi_x = 0$  is the constraint of the tangent space at  $x \in \mathcal{M}$  to be projected onto, then the projection matrix  $\mathbf{P}_x$  is derived as*

$$\mathbf{P}_x = -\mathbf{A}^T(\mathbf{A}\mathbf{A}^T)^{-1}\mathbf{A} + \mathbf{I}.$$

It should be noted that  $\mathbf{P}_x$  is *symmetric*.

Now, we provide the proof of Theorem 4.4.

*Proof of Theorem 4.4.* For simplicity, we assume that the parameter  $x_t$  represents its vectorized form throughout the analysis below. We also assume that the Riemannian stochastic gradients  $\text{grad}f_{i_t}(x_t)$  and the Riemannian gradient  $\text{grad}f(x_t)$  at  $x_t$  represent their vectorized forms of their original matrix forms, which are  $\mathbf{g}_t(x_t)$  and  $\mathbf{g}(x_t)$ , respectively. Accordingly, we assume a projection matrix  $\mathbf{P}_{x_t}$  as in Lemma A.1 as the projection operator  $\mathcal{P}_{x_t}$ .

Since  $f$  is retraction  $L$ -smooth in Lemma 4.2, we have

$$f(x_{t+1}) \leq f(x_t) + \langle \mathbf{g}(x_t), -\alpha_t \mathbf{P}_{x_t} \hat{\mathbf{V}}_t^{-1/2} \mathbf{g}_t(x_t) \rangle_2 + \frac{L}{2} \| -\alpha_t \mathbf{P}_{x_t} \hat{\mathbf{V}}_t^{-1/2} \mathbf{g}_t(x_t) \|_2^2. \quad (\text{A.1})$$

We first bound the second term in the right hand side of above. Here, we notice that

$$\begin{aligned} \langle \mathbf{g}(x_t), \mathbf{P}_{x_t} \hat{\mathbf{V}}_t^{-1/2} \mathbf{g}_t(x_t) \rangle_2 &= \langle \mathbf{P}_{x_t} \mathbf{g}(x_t), \hat{\mathbf{V}}_t^{-1/2} \mathbf{g}_t(x_t) \rangle_2 \\ &= \langle \mathbf{g}(x_t), \hat{\mathbf{V}}_t^{-1/2} \mathbf{g}_t(x_t) \rangle_2, \end{aligned}$$

where the first equality holds because  $\mathbf{P}_{x_t}$  is symmetric as stated at Lemma A.1 and the second equality holds because  $\mathbf{g}_t(x_t)$  is on the tangent space and  $\mathbf{P}_{x_t} \mathbf{g}_t(x_t)$  is just  $\mathbf{g}_t(x_t)$ . This observation can be also obtained by noticing  $\mathbf{P}_{x_t} = -\mathbf{Q}_t + \mathbf{I}$ , where  $\mathbf{Q} = \mathbf{A}^T(\mathbf{A}\mathbf{A}^T)^{-1}\mathbf{A}$  in Lemma A.1, as presented below.

$$\begin{aligned} \langle \mathbf{g}(x_t), (-\mathbf{Q}_t + \mathbf{I}) \hat{\mathbf{V}}_t^{-1/2} \mathbf{g}_t(x_t) \rangle_2 &= \langle \mathbf{g}(x_t), -\mathbf{Q}_t \hat{\mathbf{V}}_t^{-1/2} \mathbf{g}_t(x_t) \rangle_2 + \langle \mathbf{g}(x_t), \hat{\mathbf{V}}_t^{-1/2} \mathbf{g}_t(x_t) \rangle_2 \\ &= \langle \mathbf{g}(x_t), \hat{\mathbf{V}}_t^{-1/2} \mathbf{g}_t(x_t) \rangle_2, \end{aligned}$$

where the second equality holds because  $-\mathbf{Q}_t \hat{\mathbf{V}}_t^{-1/2} \mathbf{g}_t(x_t)$  belongs to the *normal space* to the tangent space  $T_{x_t}\mathcal{M}$ , and its inner product with the tangent vector  $\mathbf{g}(x_t) \in T_{x_t}\mathcal{M}$  is zero. We can also bound the third term of (A.1) as

$$\frac{L}{2} \| -\alpha_t \mathbf{P}_{x_t} \hat{\mathbf{V}}_t^{-1/2} \mathbf{g}_t(x_t) \|_2^2 \leq \frac{L}{2} \| \alpha_t \hat{\mathbf{V}}_t^{-1/2} \mathbf{g}_t(x_t) \|_2^2,$$

where the inequality holds because of the contraction of the projection operator.

Consequently, (A.1) results in

$$f(x_{t+1}) \leq f(x_t) + \langle \mathbf{g}(x_t), -\alpha_t \hat{\mathbf{V}}_t^{-1/2} \mathbf{g}_t(x_t) \rangle_2 + \frac{L}{2} \| \alpha_t \hat{\mathbf{V}}_t^{-1/2} \mathbf{g}_t(x_t) \|_2^2. \quad (\text{A.2})$$

Now, we consider the case (A.2) with  $t = 1$ . We have

$$f(x_2) \leq f(x_1) + \langle \mathbf{g}(x_1), -\alpha_1 \hat{\mathbf{V}}_1^{-1/2} \mathbf{g}_1(x_1) \rangle_2 + \frac{L}{2} \| \alpha_1 \hat{\mathbf{V}}_1^{-1/2} \mathbf{g}_1(x_1) \|_2^2.$$

Taking expectation and rearranging terms of above yields

$$\begin{aligned} \mathbb{E}_{i_1}[f(x_2)] &\leq \mathbb{E}_{i_1}[f(x_1)] + \mathbb{E}_{i_1}[\langle \mathbf{g}(x_1), -\alpha_1 \hat{\mathbf{V}}_1^{-1/2} \mathbf{g}_1(x_1) \rangle_2] + \mathbb{E}_{i_1} \left[ \frac{L}{2} \| \alpha_1 \hat{\mathbf{V}}_1^{-1/2} \mathbf{g}_1(x_1) \|_2^2 \right] \\ &= f(x_1) + \mathbb{E}_{i_1} \left[ \left\langle \mathbf{g}(x_1), -\alpha_1 \frac{\mathbf{g}_1(x_1)}{\sqrt{\hat{\mathbf{v}}_1}} \right\rangle_2 \right] + \mathbb{E}_{i_1} \left[ \frac{L}{2} \left\| \frac{\alpha_1 \mathbf{g}_1(x_1)}{\sqrt{\hat{\mathbf{v}}_1}} \right\|_2^2 \right]. \quad (\text{A.3}) \end{aligned}$$

Next, we consider the case (A.2) with  $t \geq 2$ . We have

$$\begin{aligned}
-\langle \mathbf{g}(x_t), \alpha_t \mathbf{P}_{x_t} \hat{\mathbf{V}}_t^{-1/2} \mathbf{g}_t(x_t) \rangle_2 &= -\langle \mathbf{g}(x_t), \alpha_t \hat{\mathbf{V}}_t^{-1/2} \mathbf{g}_t(x_t) \rangle_2 \\
&= -\langle \mathbf{g}(x_t), \alpha_{t-1} \hat{\mathbf{V}}_{t-1}^{-1/2} \mathbf{g}_t(x_t) \rangle_2 \\
&\quad -\langle \mathbf{g}(x_t), \alpha_t \hat{\mathbf{V}}_t^{-1/2} \mathbf{g}_t(x_t) \rangle_2 + \langle \mathbf{g}(x_t), \alpha_{t-1} \hat{\mathbf{V}}_{t-1}^{-1/2} \mathbf{g}_t(x_t) \rangle_2 \\
&= -\langle \mathbf{g}(x_t), \alpha_{t-1} \hat{\mathbf{V}}_{t-1}^{-1/2} \mathbf{g}_t(x_t) \rangle_2 - \langle \mathbf{g}(x_t), (\alpha_t \hat{\mathbf{V}}_t^{-1/2} - \alpha_{t-1} \hat{\mathbf{V}}_{t-1}^{-1/2}) \mathbf{g}_t(x_t) \rangle_2 \\
&\leq -\langle \mathbf{g}(x_t), \alpha_{t-1} \hat{\mathbf{V}}_{t-1}^{-1/2} \mathbf{g}_t(x_t) \rangle_2 + H^2 \left[ \sum_{j=1}^d \left| \frac{\alpha_t}{\sqrt{(\hat{\mathbf{v}}_t)_j}} - \frac{\alpha_{t-1}}{\sqrt{(\hat{\mathbf{v}}_{t-1})_j}} \right| \right],
\end{aligned} \tag{A.4}$$

where the inequality holds because of Assumption 1 (1.3) and Lemma 4.3.

Plugging (A.4) into (A.2) yields

$$\begin{aligned}
f(x_{t+1}) &\leq f(x_t) - \langle \mathbf{g}(x_t), \alpha_{t-1} \hat{\mathbf{V}}_{t-1}^{-1/2} \mathbf{g}_t(x_t) \rangle_2 \\
&\quad + H^2 \left[ \sum_{j=1}^d \left| \frac{\alpha_t}{\sqrt{(\hat{\mathbf{v}}_t)_j}} - \frac{\alpha_{t-1}}{\sqrt{(\hat{\mathbf{v}}_{t-1})_j}} \right| \right] + \frac{L}{2} \left\| \frac{\alpha_t \mathbf{g}_t(x_t)}{\sqrt{\hat{\mathbf{v}}_t}} \right\|_2^2.
\end{aligned}$$

Taking expectation and rearranging terms, we have

$$\begin{aligned}
\mathbb{E}_{i_t}[f(x_{t+1})] &\leq \mathbb{E}_{i_t}[f(x_t)] - \mathbb{E}_{i_t} \left[ \langle \mathbf{g}(x_t), \alpha_{t-1} \hat{\mathbf{V}}_{t-1}^{-1/2} \mathbf{g}_t(x_t) \rangle_2 \right] \\
&\quad + H^2 \mathbb{E}_{i_t} \left[ \sum_{j=1}^d \left| \frac{\alpha_t}{\sqrt{(\hat{\mathbf{v}}_t)_j}} - \frac{\alpha_{t-1}}{\sqrt{(\hat{\mathbf{v}}_{t-1})_j}} \right| \right] + \mathbb{E}_{i_t} \left[ \frac{L}{2} \left\| \frac{\alpha_t \mathbf{g}_t(x_t)}{\sqrt{\hat{\mathbf{v}}_t}} \right\|_2^2 \right], \\
&\leq f(x_t) - \langle \mathbf{g}(x_t), \alpha_{t-1} \hat{\mathbf{V}}_{t-1}^{-1/2} \mathbb{E}_{i_t}[\mathbf{g}_t(x_t)] \rangle_2 \\
&\quad + H^2 \mathbb{E}_{i_t} \left[ \sum_{j=1}^d \left| \frac{\alpha_t}{\sqrt{(\hat{\mathbf{v}}_t)_j}} - \frac{\alpha_{t-1}}{\sqrt{(\hat{\mathbf{v}}_{t-1})_j}} \right| \right] + \mathbb{E}_{i_t} \left[ \frac{L}{2} \left\| \frac{\alpha_t \mathbf{g}_t(x_t)}{\sqrt{\hat{\mathbf{v}}_t}} \right\|_2^2 \right], \\
&= f(x_t) - \alpha_{t-1} \left\langle \mathbf{g}(x_t), \frac{\mathbf{g}(x_t)}{\sqrt{\hat{\mathbf{v}}_{t-1}}} \right\rangle_2 \\
&\quad + H^2 \mathbb{E}_{i_t} \left[ \sum_{j=1}^d \left| \frac{\alpha_t}{\sqrt{(\hat{\mathbf{v}}_t)_j}} - \frac{\alpha_{t-1}}{\sqrt{(\hat{\mathbf{v}}_{t-1})_j}} \right| \right] + \mathbb{E}_{i_t} \left[ \frac{L}{2} \left\| \frac{\alpha_t \mathbf{g}_t(x_t)}{\sqrt{\hat{\mathbf{v}}_t}} \right\|_2^2 \right],
\end{aligned}$$

Rearranging above, we obtain

$$\begin{aligned}
&\alpha_{t-1} \left\langle \mathbf{g}(x_t), \frac{\mathbf{g}(x_t)}{\sqrt{\hat{\mathbf{v}}_{t-1}}} \right\rangle_2 \\
&\leq \mathbb{E}_{i_t} \left[ \frac{L}{2} \left\| \frac{\alpha_t \mathbf{g}_t(x_t)}{\sqrt{\hat{\mathbf{v}}_t}} \right\|_2^2 \right] + H^2 \mathbb{E}_{i_t} \left[ \sum_{j=1}^d \left| \frac{\alpha_t}{\sqrt{(\hat{\mathbf{v}}_t)_j}} - \frac{\alpha_{t-1}}{\sqrt{(\hat{\mathbf{v}}_{t-1})_j}} \right| \right] + f(x_t) - \mathbb{E}_{i_t}[f(x_{t+1})].
\end{aligned} \tag{A.5}$$

After taking the expectation of each side with respect to  $i_{t-1}, \dots, i_2, i_1$  and telescoping (A.5) for  $t = 2$  to  $T$  and adding (A.3), we have

$$\begin{aligned}
& \mathbb{E} \left[ \sum_{t=2}^T \alpha_{t-1} \left\langle \mathbf{g}(x_t), \frac{\mathbf{g}(x_t)}{\sqrt{\hat{\mathbf{v}}_{t-1}}} \right\rangle_2 \right] \\
& \leq \mathbb{E} \left[ \frac{L}{2} \sum_{t=2}^T \left\| \frac{\alpha_t \mathbf{g}_t(x_t)}{\sqrt{\hat{\mathbf{v}}_t}} \right\|_2^2 \right] + H^2 \mathbb{E} \left[ \sum_{t=2}^T \sum_{j=1}^d \left| \frac{\alpha_t}{\sqrt{(\hat{\mathbf{v}}_t)_j}} - \frac{\alpha_{t-1}}{\sqrt{(\hat{\mathbf{v}}_{t-1})_j}} \right| \right] + \mathbb{E} \left[ \sum_{t=2}^T (f(x_t) - f(x_{t+1})) \right] \\
& \quad + \mathbb{E} \left[ f(x_1) - \mathbb{E}_{i_1}[f(x_2)] + \left\langle \mathbf{g}(x_1), -\alpha_1 \frac{\mathbf{g}(x_1)}{\sqrt{\hat{\mathbf{v}}_1}} \right\rangle_2 + \mathbb{E}_{i_1} \left[ \frac{L}{2} \left\| \frac{\alpha_1 \mathbf{g}_1(x_1)}{\sqrt{\hat{\mathbf{v}}_1}} \right\|_2^2 \right] \right] \\
& = \mathbb{E} \left[ \frac{L}{2} \sum_{t=1}^T \left\| \frac{\alpha_t \mathbf{g}_t(x_t)}{\sqrt{\hat{\mathbf{v}}_t}} \right\|_2^2 + H^2 \sum_{t=2}^T \left\| \frac{\alpha_t}{\sqrt{\hat{\mathbf{v}}_t}} - \frac{\alpha_{t-1}}{\sqrt{\hat{\mathbf{v}}_{t-1}}} \right\|_1 + \left\langle \mathbf{g}(x_1), -\alpha_1 \frac{\mathbf{g}_1(x_1)}{\sqrt{\hat{\mathbf{v}}_1}} \right\rangle_2 \right] + \mathbb{E}[f(x_1) - f(x^*)],
\end{aligned} \tag{A.6}$$

where  $x^*$  is an optimal of  $f$ . The terms  $\mathbb{E} \left[ \left\langle \mathbf{g}(x_1), -\alpha_1 \frac{\mathbf{g}_1(x_1)}{\sqrt{\hat{\mathbf{v}}_1}} \right\rangle_2 \right] + \mathbb{E}[f(x_1) - f(x^*)]$  in (A.6) do not depend on  $T$  and hence are constants, which we call  $C$ . This completes the proof.  $\square$

### A.3 Proof of Corollary 4.5

This section provides the complete proof of Corollary 4.5.

*Proof of Corollary 4.5.* From the assumption, the first term in the right-hand side of (A.6) yields

$$\begin{aligned}
& \mathbb{E} \left[ \frac{L}{2} \sum_{t=1}^T \left\| \frac{\alpha_t \mathbf{g}_t(x_t)}{\sqrt{\hat{\mathbf{v}}_t}} \right\|_2^2 \right] \leq \mathbb{E} \left[ \frac{L}{2} \sum_{t=1}^T \left\| \frac{\alpha_t \mathbf{g}_t(x_t)}{c} \right\|_2^2 \right] \\
& \leq \mathbb{E} \left[ \frac{L}{2} \sum_{t=1}^T \left( \frac{1}{c\sqrt{t}} \right)^2 \|\mathbf{g}_t(x_t)\|_2^2 \right] \leq \frac{LH^2}{2c^2} \sum_{t=1}^T \frac{1}{t} \leq \frac{LH^2}{2c^2} (1 + \log T),
\end{aligned} \tag{A.7}$$

where the last inequality uses  $\sum_{t=1}^T \frac{1}{t} \leq 1 + \log T$ .

The second term in the right-hand side of (A.6) yields

$$\begin{aligned}
& H^2 \mathbb{E} \left[ \sum_{t=2}^T \left\| \frac{\alpha_t}{\sqrt{\hat{\mathbf{v}}_t}} - \frac{\alpha_{t-1}}{\sqrt{\hat{\mathbf{v}}_{t-1}}} \right\|_1 \right] = H^2 \mathbb{E} \left[ \sum_{t=2}^T \sum_{j=1}^d \left( \frac{\alpha_{t-1}}{\sqrt{(\hat{\mathbf{v}}_{t-1})_j}} - \frac{\alpha_t}{\sqrt{(\hat{\mathbf{v}}_t)_j}} \right) \right] \\
& = H^2 \mathbb{E} \left[ \sum_{j=1}^d \left( \frac{\alpha_1}{\sqrt{(\hat{\mathbf{v}}_1)_j}} - \frac{\alpha_T}{\sqrt{(\hat{\mathbf{v}}_T)_j}} \right) \right] \leq H^2 \mathbb{E} \left[ \sum_{j=1}^d \frac{\alpha_1}{\sqrt{(\hat{\mathbf{v}}_1)_j}} \right] \leq \frac{dH^2}{c},
\end{aligned} \tag{A.8}$$

where the first equality holds because of  $(\hat{\mathbf{v}}_t)_j \geq (\hat{\mathbf{v}}_{t-1})_j$  and  $\alpha_t \leq \alpha_{t-1}$ .

The third term in the right-hand side of (A.6) with  $\alpha_1 = 1$  yields

$$\mathbb{E} \left[ \left\langle \mathbf{g}(x_1), -\alpha_1 \frac{\mathbf{g}_1(x_1)}{\sqrt{\hat{\mathbf{v}}_1}} \right\rangle_2 \right] \leq H^2 \sum_{j=1}^d \frac{1}{\sqrt{(\hat{\mathbf{v}}_1)_j}} \leq \frac{dH^2}{c}. \tag{A.9}$$

Then, plugging (A.7), (A.8) and (A.9) into (A.6) yields

$$\mathbb{E} \left[ \sum_{t=2}^T \alpha_{t-1} \left\langle \mathbf{g}(x_t), \frac{\mathbf{g}(x_t)}{\sqrt{\hat{\mathbf{v}}_{t-1}}} \right\rangle_2 \right] \leq \frac{LH^2}{2c^2} (1 + \log T) + \frac{2dH^2}{c} + \mathbb{E}[f(x_1) - f(x^*)]. \quad (\text{A.10})$$

Here, from  $\alpha_t = 1/\sqrt{t}$  and  $(\hat{\mathbf{v}}_t)_j \leq H^2$  in Lemma, we have

$$\frac{\alpha_{t-1}}{(\sqrt{\hat{\mathbf{v}}_{t-1}})_j} \geq \frac{1}{H\sqrt{t-1}}.$$

Therefore, we obtain

$$\begin{aligned} \mathbb{E} \left[ \sum_{t=2}^T \alpha_{t-1} \left\langle \mathbf{g}(x_t), \frac{\mathbf{g}(x_t)}{\sqrt{\hat{\mathbf{v}}_{t-1}}} \right\rangle_2 \right] &\geq \mathbb{E} \left[ \sum_{t=2}^T \frac{1}{H\sqrt{t-1}} \|\mathbf{g}(x_t)\|_2^2 \right] \\ &\geq \sum_{t=2}^T \frac{1}{H\sqrt{t-1}} \min_{t \in [2, \dots, T]} \mathbb{E} \left[ \|\mathbf{g}(x_t)\|_2^2 \right] \\ &= \frac{\min_{t \in [2, \dots, T]} \mathbb{E}[\|\mathbf{g}(x_t)\|_2^2]}{H} \sum_{t=2}^T \frac{1}{\sqrt{t-1}} \\ &\geq \frac{\sqrt{T-1}}{H} \min_{t \in [2, \dots, T]} \mathbb{E}[\|\mathbf{g}(x_t)\|_2^2], \end{aligned} \quad (\text{A.11})$$

where the third equality holds due to  $\sum_{t=1}^T \frac{1}{\sqrt{t}} \geq \sqrt{T}$ .

Hence, plugging (A.11) into (A.10) and arranging it, we have

$$\min_{t \in [2, \dots, T]} \mathbb{E}[\|\mathbf{g}(x_t)\|_2^2] \leq \frac{1}{\sqrt{T-1}} \left[ \frac{LH^3}{2c^2} (1 + \log T) + \frac{2dH^3}{c} + H\mathbb{E}[f(x_1) - f(x^*)] \right]. \quad (\text{A.12})$$

Rearranging (A.14) and addressing the original definition  $\mathbf{g}(x) := \text{vec}(\text{grad}f(x))$ , we finally obtain

$$\min_{t \in [2, \dots, T]} \mathbb{E} \|\text{grad}f(x_t)\|_F^2 \leq \frac{1}{\sqrt{T-1}} (Q_1 + Q_2 \log(T)),$$

where  $\{Q_i\}_{i=1}^2$  are defined as below:

$$\begin{aligned} Q_1 &= \frac{LH^3}{2c^2} + \frac{2dH^3}{c} + H\mathbb{E}[f(x_1) - f(x^*)], \\ Q_2 &= \frac{LH^3}{2c^2}. \end{aligned}$$

This completes the proof.  $\square$

#### A.4 Variable $\beta$ algorithm and its convergence analysis (not included in the main manuscript)

We consider a variant of Algorithm 1, which uses  $\beta = 1 - 1/t$ , and give its convergence analysis. For this purpose, we additionally modify Algorithm 1 to make the proof simpler, where the max operator is directly performed onto  $\mathbf{v}_t$  instead of  $\mathbf{l}_t$  and  $\mathbf{r}_t$  individually. This ensures  $(\hat{\mathbf{v}}_t)_j \geq (\hat{\mathbf{v}}_{t-1})_j$ , and enables to directly apply the result of Lemma A.2 for (A.13) of the proof of Corollary A.3 as well as similarly in (A.8) of the proof of Corollary 4.5. As shown later, its convergence rate is slightly better than that of Algorithm 1. The new algorithm is summarized in Algorithm A.1.

---

##### Algorithm A.1 Riemannian adaptive stochastic algorithm with variable $\beta$

---

**Require:** Step size  $\{\alpha_t\}_{t=1}^T$ .

- 1: Initialize  $x_1 \in \mathcal{M}$ ,  $\mathbf{v}_0 = \hat{\mathbf{v}}_0 = \mathbf{0}_n$ .
  - 2: **for**  $t = 1, 2, \dots, T$  **do**
  - 3:   Set  $\beta = 1 - 1/t$ .
  - 4:   Compute Riemannian stochastic gradient  $\mathbf{G}_t = \text{grad}f_t(x_t)$ .
  - 5:   Compute  $\mathbf{p}_t = \text{diag}(\mathbf{G}_t \mathbf{G}_t^T)/r$  and  $\mathbf{q}_t = \text{diag}(\mathbf{G}_t^T \mathbf{G}_t)/n$ .
  - 6:   Modify  $\mathbf{p}_t$  and  $\mathbf{q}_t$  to  $\hat{\mathbf{p}}_t$  and  $\hat{\mathbf{q}}_t$  to satisfy Assumption 2.
  - 7:   Update  $\mathbf{l}_t = \beta \mathbf{l}_{t-1} + (1 - \beta) \hat{\mathbf{p}}_t$ .
  - 8:   Update  $\mathbf{r}_t = \beta \mathbf{r}_{t-1} + (1 - \beta) \hat{\mathbf{q}}_t$ .
  - 9:   Calculate  $\mathbf{v}_t = \mathbf{r}_t^{1/2} \otimes \mathbf{l}_t^{1/2}$ .
  - 10:   Calculate  $\hat{\mathbf{v}}_t = \max(\hat{\mathbf{v}}_{t-1}, \mathbf{v}_t)$ .
  - 11:    $x_{t+1} = R_{x_t}(-\alpha_t \mathcal{P}_{x_t}(\text{vec}^{-1}(\text{Diag}(\hat{\mathbf{v}}_t)^{-1/2} \text{vec}(\mathbf{G}_t))))$ .
  - 12: **end for**
- 

It should be noted that the modified algorithm explicitly generates  $\hat{\mathbf{v}}_t$ , and this causes computational inefficiency. It should be also noted that we need to modify  $\mathbf{p}_t = \text{diag}(\mathbf{G}_t \mathbf{G}_t^T)/r$  and  $\mathbf{q}_t = \text{diag}(\mathbf{G}_t^T \mathbf{G}_t)/n$  into  $\hat{\mathbf{p}}_t$  and  $\hat{\mathbf{q}}_t$  to guarantee Assumption 2 as described in Step 6 of Algorithm A.1.

An additional assumption is first required.

**Assumption 2.** We denote  $\text{grad}f_{i_t}(x_t)$  as  $\mathbf{G}_t \in \mathbb{R}^{n \times r}$ , and the vectorized form of  $\text{grad}f_{i_t}(x_t)$  as  $\mathbf{g}_t(x_t) \in \mathbb{R}^{nr}$ . Then, we assume

$$\sqrt{(\text{diag}(\mathbf{G}_t^T \mathbf{G}_t))_p (\text{diag}(\mathbf{G}_t \mathbf{G}_t^T))_q / (nr)} \geq (\mathbf{g}_t(x_t))_j^2,$$

where  $j = n(p-1) + q$  with  $p \in [r]$  and  $q \in [n]$ .

Next, we derive the condition of the sequence of  $\mathbf{v}_t$  below.

**Lemma A.2.** Let  $\{x_t\}$  and  $\{\mathbf{v}_t\}$  be the sequences obtained from Algorithm A.1 with  $\beta = 1 - 1/t$ . Under Assumptions 1 and 2, the sequence  $\{\mathbf{v}_t\}$  satisfies

$$(\mathbf{v}_t)_j \geq \frac{1}{t} \sum_{i=1}^t (\mathbf{g}_i(x_i))_j^2,$$

where  $(\mathbf{g}_i(x_i))_j$  is the  $j$ -th element of the vectorized stochastic gradient  $\mathbf{g}_i(x_i)$ .



*Proof.* From  $\beta = 1 - \frac{1}{t}$  in Algorithm A.1, we have

$$\begin{aligned}\mathbf{l}_t &= \left(1 - \frac{1}{t}\right) \mathbf{l}_{t-1} + \frac{1}{t} \frac{\text{diag}(\mathbf{G}_t \mathbf{G}_t^T)}{r}, \\ \mathbf{r}_t &= \left(1 - \frac{1}{t}\right) \mathbf{r}_{t-1} + \frac{1}{t} \frac{\text{diag}(\mathbf{G}_t^T \mathbf{G}_t)}{n}.\end{aligned}$$

Addressing the  $j$ -th element of  $\mathbf{v}_t = \mathbf{r}_t^{1/2} \otimes \mathbf{l}_t^{1/2} \in \mathbb{R}^{nr}$ , denoted as  $(\mathbf{v}_t)_j \in \mathbb{R}$ , we have

$$\begin{aligned}(\mathbf{v}_t)_j &= (\mathbf{r}_t^{1/2} \otimes \mathbf{l}_t^{1/2})_j \\ &= \left[ \left( \frac{t-1}{t} \mathbf{r}_{t-1} + \frac{1}{t} \frac{\text{diag}(\mathbf{G}_t^T \mathbf{G}_t)}{n} \right)_p \right]^{1/2} \left[ \left( \frac{t-1}{t} \mathbf{l}_{t-1} + \frac{1}{t} \frac{\text{diag}(\mathbf{G}_t \mathbf{G}_t^T)}{r} \right)_q \right]^{1/2} \\ &= \left[ \left( \frac{t-1}{t} \mathbf{r}_{t-1} + \frac{1}{t} \frac{\text{diag}(\mathbf{G}_t^T \mathbf{G}_t)}{n} \right)_p \left( \frac{t-1}{t} \mathbf{l}_{t-1} + \frac{1}{t} \frac{\text{diag}(\mathbf{G}_t \mathbf{G}_t^T)}{r} \right)_q \right]^{1/2} \\ &= \left[ \left( \frac{t-1}{t} (\mathbf{r}_{t-1})_p + \frac{1}{t} \frac{(\text{diag}(\mathbf{G}_t^T \mathbf{G}_t))_p}{n} \right) \left( \frac{t-1}{t} (\mathbf{l}_{t-1})_q + \frac{1}{t} \frac{(\text{diag}(\mathbf{G}_t \mathbf{G}_t^T))_q}{r} \right) \right]^{1/2} \\ &= \left[ \left( \frac{t-1}{t} \right)^2 (\mathbf{r}_{t-1})_p (\mathbf{l}_{t-1})_q + \left( \frac{1}{t} \right)^2 \frac{(\text{diag}(\mathbf{G}_t^T \mathbf{G}_t))_p (\text{diag}(\mathbf{G}_t \mathbf{G}_t^T))_q}{nr} \right. \\ &\quad \left. + \frac{1}{t} \left(1 - \frac{1}{t}\right) (\mathbf{r}_{t-1})_p \frac{(\text{diag}(\mathbf{G}_t \mathbf{G}_t^T))_q}{r} + \frac{1}{t} \left(1 - \frac{1}{t}\right) (\mathbf{l}_{t-1})_q \frac{(\text{diag}(\mathbf{G}_t^T \mathbf{G}_t))_p}{n} \right]^{1/2} \\ &= \left[ \left( \frac{t-1}{t} \right)^2 (\mathbf{r}_{t-1})_p (\mathbf{l}_{t-1})_q + \left( \frac{1}{t} \right)^2 \frac{(\text{diag}(\mathbf{G}_t^T \mathbf{G}_t))_p (\text{diag}(\mathbf{G}_t \mathbf{G}_t^T))_q}{nr} \right. \\ &\quad \left. + \frac{1}{t} \left(1 - \frac{1}{t}\right) \left[ (\mathbf{r}_{t-1})_p \frac{(\text{diag}(\mathbf{G}_t \mathbf{G}_t^T))_q}{r} + (\mathbf{l}_{t-1})_q \frac{(\text{diag}(\mathbf{G}_t^T \mathbf{G}_t))_p}{n} \right] \right]^{1/2} \\ &\geq \left[ \left( \frac{t-1}{t} \right)^2 (\mathbf{r}_{t-1})_p (\mathbf{l}_{t-1})_q + \left( \frac{1}{t} \right)^2 \frac{(\text{diag}(\mathbf{G}_t^T \mathbf{G}_t))_p (\text{diag}(\mathbf{G}_t \mathbf{G}_t^T))_q}{nr} \right. \\ &\quad \left. + \frac{2}{t} \left(1 - \frac{1}{t}\right) \sqrt{(\mathbf{r}_{t-1})_p \frac{(\text{diag}(\mathbf{G}_t \mathbf{G}_t^T))_q}{n}} \sqrt{(\mathbf{l}_{t-1})_q \frac{(\text{diag}(\mathbf{G}_t^T \mathbf{G}_t))_p}{r}} \right]^{1/2} \\ &= \left( \frac{t-1}{t} \right) \sqrt{(\mathbf{r}_{t-1})_p (\mathbf{l}_{t-1})_q} + \frac{1}{t} \sqrt{\frac{(\text{diag}(\mathbf{G}_t^T \mathbf{G}_t))_p (\text{diag}(\mathbf{G}_t \mathbf{G}_t^T))_q}{nr}},\end{aligned}$$

where the inequality uses the inequality of arithmetic and geometric means. Since  $(\mathbf{v}_{t-1})_j = (\mathbf{r}_{t-1}^{1/2} \otimes \mathbf{l}_{t-1}^{1/2})_j = \sqrt{(\mathbf{r}_{t-1})_p (\mathbf{l}_{t-1})_q}$ , we finally have

$$(\mathbf{v}_t)_j \geq \left(1 - \frac{1}{t}\right) (\mathbf{v}_{t-1})_j + \frac{1}{t} \sqrt{\frac{(\text{diag}(\mathbf{G}_t^T \mathbf{G}_t))_p (\text{diag}(\mathbf{G}_t \mathbf{G}_t^T))_q}{nr}}.$$

Consequently, from Assumption 2, and  $(\mathbf{v}_0) = \mathbf{0}$ , the recursive updates of the inequality above finally lead to

$$\begin{aligned}
(\mathbf{v}_t)_j &\geq \left(1 - \frac{1}{t}\right) (\mathbf{v}_{t-1})_j + \frac{1}{t} (\mathbf{g}_t(x_t))_j^2 \\
&\geq \left(1 - \frac{1}{t}\right) \left( \left(1 - \frac{1}{t-1}\right) (\mathbf{v}_{t-2})_j + \frac{1}{t-1} (\mathbf{g}_{t-1}(x_{t-1}))_j^2 \right) + \frac{1}{t} (\mathbf{g}_t(x_t))_j^2 \\
&\geq \frac{1}{t} \sum_{i=1}^t (\mathbf{g}_i(x_i))_j^2.
\end{aligned}$$

This yields the desired result, and this completes the proof.  $\square$

Now, we derive an convergence rate of Algorithm A.1 below.

**Corollary A.3** (Convergence rate analysis of Algorithm A.1). *Let  $\{x_t\}$  and  $\{\hat{\mathbf{v}}_t\}$  be the sequences obtained from Algorithm A.1. Suppose  $\alpha_t = 1/\sqrt{t}$ , and, suppose that  $\min_{j \in [d]} \sqrt{(\hat{\mathbf{v}}_1)_j}$  is lower-bounded by a constant  $c > 0$ , where  $d$  is the dimension of the manifold  $\mathcal{M}$ . Also, suppose that Lemma A.2 holds. Then, under Assumptions 1 and 2, the output of  $x_t$  of Algorithm A.1 satisfies*

$$\min_{t \in [2, \dots, T]} \mathbb{E} \|\text{grad} f(x_t)\|_F^2 \leq \frac{1}{\sqrt{T-1}} (R_1 + R_2 \log(T)),$$

where

$$\begin{aligned}
R_1 &= \frac{dLH}{2} (1 + 2 \log H) + \frac{2dH^3}{c} + H \mathbb{E}[f(x_1) - f(x^*)], \\
R_2 &= \frac{LH^3}{2c^2}.
\end{aligned}$$

As seen, the constant  $R_1$  is less than  $Q_1$  in Corollary 4.5.

We provide the complete proof of Corollary A.3.

*Proof of Corollary A.3.* From the assumptions  $\alpha_t = 1/\sqrt{t}$  and  $\sqrt{(\text{diag}(\mathbf{G}_t^T \mathbf{G}_t))_p (\text{diag}(\mathbf{G}_t \mathbf{G}_t^T))_q / nr} \geq (\mathbf{g}_t(x_t))_j^2$  in Assumption 2, and Lemma A.2, we obtain

$$\frac{\alpha_t}{\sqrt{(\hat{\mathbf{v}}_t)_j}} \leq \frac{1}{\sqrt{t(\mathbf{v}_t)_j}} \leq \frac{1}{\sqrt{\sum_{i=1}^t (\mathbf{g}_i(x_i))_j^2}}. \tag{A.13}$$

Therefore, the first term in the right-hand side of (A.6) yields

$$\begin{aligned}
\mathbb{E} \left[ \frac{L}{2} \sum_{t=1}^T \left\| \frac{\alpha_t \mathbf{g}_t(x_t)}{\sqrt{\hat{\mathbf{v}}_t}} \right\|_2^2 \right] &\leq \mathbb{E} \left[ \frac{L}{2} \sum_{j=1}^d \sum_{t=1}^T \frac{(\mathbf{g}_t(x_t))_j^2}{\sum_{i=1}^t (\mathbf{g}_i(x_i))_j^2} \right] \\
&\leq \mathbb{E} \left[ \frac{L}{2} \sum_{j=1}^d \left( 1 + \log \sum_{i=1}^T (\mathbf{g}_i(x_i))_j^2 \right) \right] \\
&\leq \frac{dL}{2} (1 + 2 \log H + \log T),
\end{aligned}$$

where the second inequality uses Lemma A.4 below.

The second and third terms in the right-hand side of (A.6) are identical to (A.8) and (A.9), respectively. Similarly to Corollary 4.5, we obtain

$$\min_{t \in [2, \dots, T]} \mathbb{E}[\|\mathbf{g}(x_t)\|_2^2] \leq \frac{1}{\sqrt{T-1}} \left[ \frac{dLH}{2}(1 + 2 \log H + \log T) + \frac{2dH^3}{c} + H\mathbb{E}[f(x_1) - f(x^*)] \right], \quad (\text{A.14})$$

where we use  $\sum_{t=2}^T \alpha_{t-1} = \sum_{t=1}^{T-1} \alpha_t$ ,  $\alpha_t = \frac{1}{\sqrt{t}}$  and  $\sum_{t=1}^T \frac{1}{\sqrt{t}} \geq \sqrt{T}$ .

Rearranging (A.14), we finally obtain

$$\min_{t \in [2, \dots, T]} \mathbb{E}\|\text{grad}f(x_t)\|_F^2 \leq \frac{1}{\sqrt{T-1}}(R_1 + R_2 \log(T)),$$

where  $\{R_i\}_{i=1}^2$  are defined as below:

$$\begin{aligned} R_1 &= \frac{dLH}{2}(1 + 2 \log H) + \frac{2dH^3}{c} + H\mathbb{E}[f(x_1) - f(x^*)], \\ R_2 &= \frac{LH^3}{2c^2}. \end{aligned}$$

This completes the proof.  $\square$

**Lemma A.4** ((Lemma 6 in (Ward et al., 2018))). *For  $a_t \leq 0$  and  $\sum_{i=1}^t a_i \neq 0$ , we have*

$$\sum_{t=1}^T \frac{a_t}{\sum_{i=1}^t a_t} \leq 1 + \log \sum_{t=1}^T a_t.$$

**Implementation details:** Lastly, it should be noted that, one naive implementation to satisfy Assumption 2 is to generate  $\hat{\mathbf{p}}_t$  and  $\hat{\mathbf{q}}_t$  is by enforcing

$$\sqrt{(\hat{\mathbf{p}}_t)_p (\hat{\mathbf{q}}_t)_q} = (\mathbf{g}_t(x_t))_j^2,$$

whenever  $\sqrt{(\mathbf{p}_t)_p (\mathbf{q}_t)_q}$  is less than  $(\mathbf{g}_t(x_t))_j^2$ . For this particular solution, there still exists freedom about how to determine  $(\hat{\mathbf{p}}_t)_p$  and  $(\hat{\mathbf{q}}_t)_q$ . One possible strategy is to set  $(\hat{\mathbf{p}}_t)_p = (\hat{\mathbf{q}}_t)_q = (\mathbf{g}_t(x_t))_j^2$ . However, since multiple modifications for one particular  $p$  or  $q$  could happen for different choices of  $j$ . Therefore, we select the highest  $(\mathbf{g}_t(x_t))_j^2$  among them for  $(\hat{\mathbf{p}}_t)_p$ , and then select  $(\mathbf{g}_t(x_t))_j^2$  for  $(\hat{\mathbf{q}}_t)_q$ , in a heuristic way.

## B Additional numerical results

### B.1 Results on synthetic datasets for the PCA problem (Case P1)

This section first gives the best-tuned results on a synthetic dataset for the PCA problem, well-conditioned case (**Case P1**). We also include an ill-conditioned case. The results are shown in Figures A.1 (a) and (b). Each result shows the optimality gap against the number of iterations as well as run-time. It should be noted that Figure A.1 (a-1) is identical to Figure 1 (a). From these

figures, we see that the proposed algorithms RASA-LR and RASA-R perform better than other algorithms. We also show all the results for each choice of the step size  $\alpha_0$  in Figures A.2 and A.3 for the well-conditioned case and the ill-conditioned cases, respectively. From the figures, in both the cases, RASA gives stably good performances, and RASA-LR yields the lowest optimality gap among all the baseline algorithms.

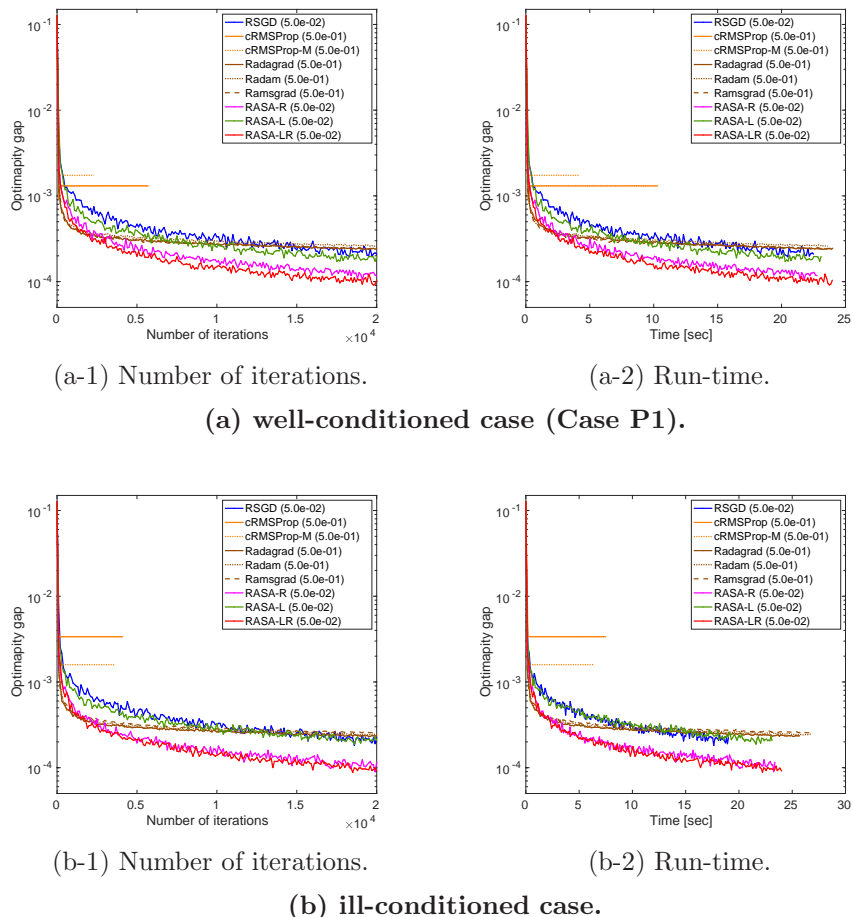


Figure A.1: Best-tuned results on synthetic datasets for the PCA problem.

## B.2 Results on the real-world datasets for the PCA problem (Case P2 and Case P3)

This section shows additional results on the real-world datasets: the MNIST dataset (**Case P2**) and the COIL100 dataset (**Case P3**). We also include the COIL20 dataset. COIL20 (Nene et al., 1996b) contains normalized 1440 camera images of the 20 objects that were taken from different angles. We use 1440 images that are resized into  $32 \times 32$  pixels. For COIL20,  $(N, n, r) = (1440, 1024, 20)$ . Figures A.4 show the best-tuned results. It should be noted that Figures A.4 (a-1) and (b-1) are identical to Figures 1 (b) and (c), respectively. As for the MNIST dataset

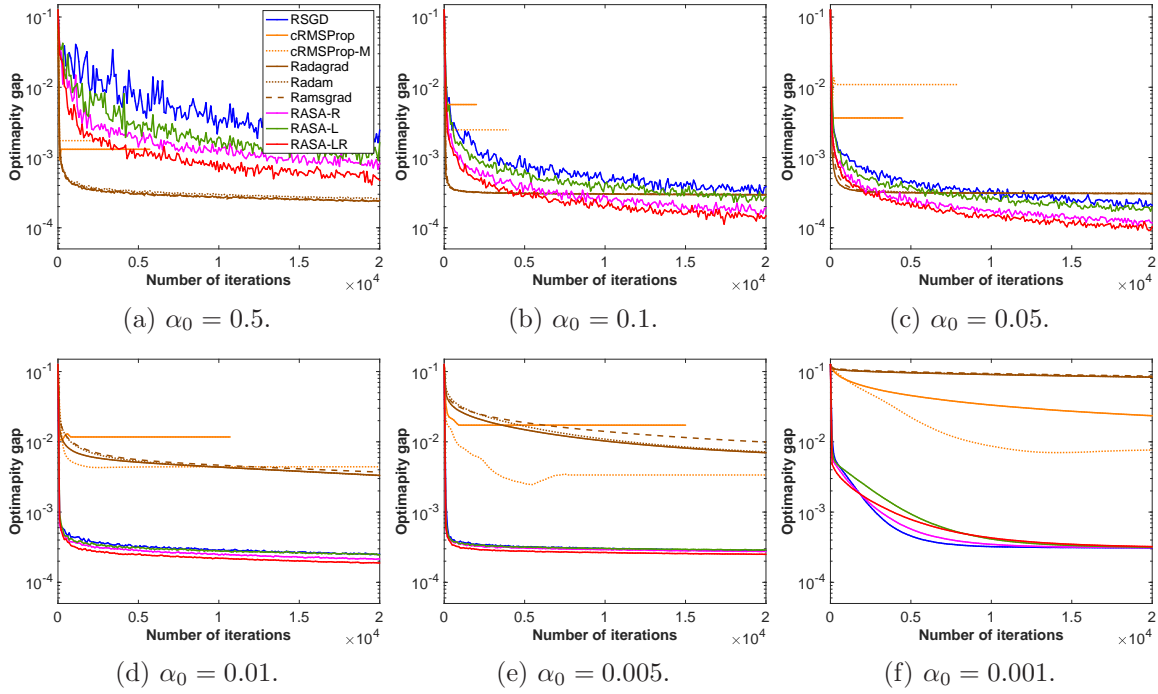


Figure A.2: Synthetic datasets on the PCA problem (well-conditioned case (**Case P1**)).

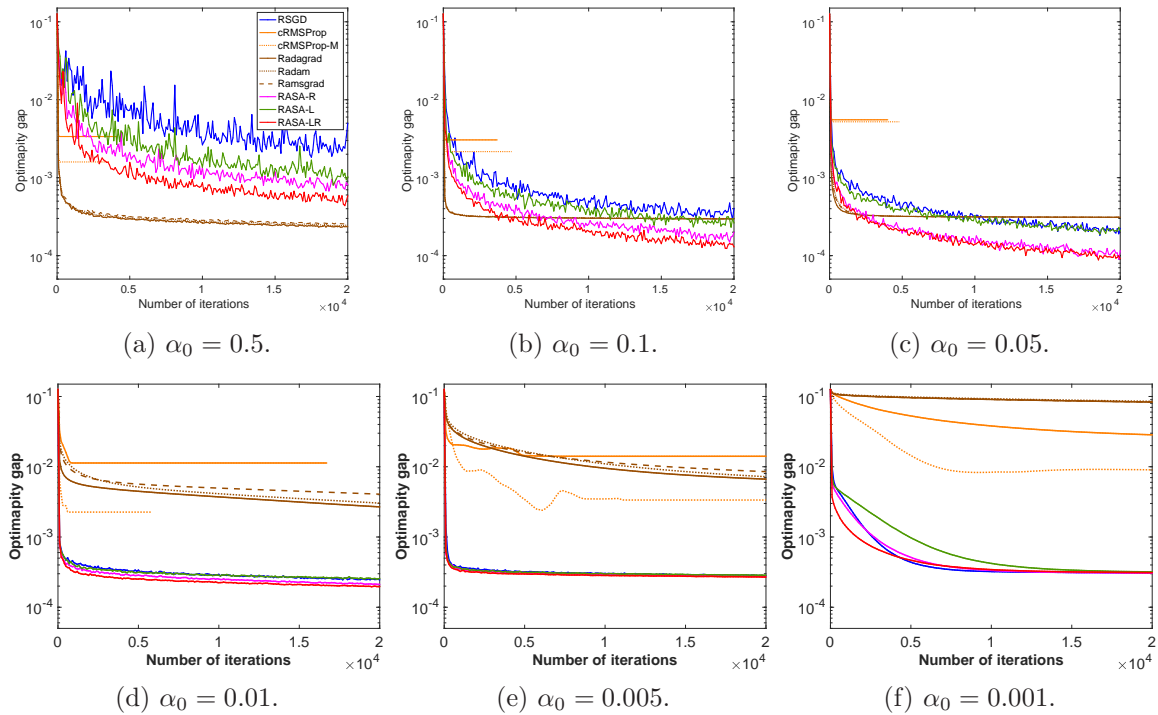


Figure A.3: Synthetic datasets on the PCA problem (ill-conditioned case).

(**Case P2**), we use  $\alpha_0 = \{5, \dots, 0.01, 0.005\}$ . As seen in the figures, Radagrad, Radam, and Ramsgrad provide better performance when  $\alpha_0 = 5$ . RASA-LR and RASA-R show their best performance when  $\alpha_0 = \{0.01, 0.05\}$ , respectively. In the COIL100 dataset (**Case P3**), we use  $\alpha_0 = \{10, \dots, 0.00001\}$ . As seen, the overall observations are similar to those in the previous datasets. We see that RASA-LR and RASA-R show their best performance among all the baseline algorithms when  $\alpha_0 = \{0.05, 0.0005\}$ , respectively. Finally, in the COIL20 dataset, we use the same range of  $\alpha_0$  as the MNIST dataset. The overall observations are almost similar to those in the previous two datasets. In summary, as the same as the synthetic datasets, RASA-LR and RASA-R stably give better performances than all the other baseline algorithms.

Additionally, we show all the results on each step size on these datasets in Figures A.5, A.6 and A.7, respectively. Lastly, in all the three datasets, we see poor performance of cRMSProp and cRMSPProp-M across difference settings.

### B.3 Results on the real-world datasets for the ICA problem (Case I1 and Case I2)

This section gives additional results of performance of the algorithms across different values of  $\alpha_0$  for **Case I1** and **Case I2**, which are shown in Figures A.8 and A.9, respectively.

### B.4 Results on the real-world datasets for the matrix completion (MC) problem

This section shows the results of the MC problems on real-world datasets.

Figures A.10(a) and (b) show the train and test root MSEs on MovieLens-1M dataset and MovieLens-10M dataset, respectively, under best-tuned step sizes. The comparison algorithms are RSGD, Radagrad, Radam, Ramsgrad and RASA-LR. From the figures, we see that RASA-LR yields best performances on all settings.

Finally, Figures A.11 (a) and (b) show the MSEs of the training set and the test set on the Jester dataset (Goldberg et al., 2001), respectively. The dataset consists of ratings of 100 jokes by 24983 users. Each rating is a real number between  $-10$  and  $10$ . The step sizes values are  $\alpha_0 = \{1, 0.1, 0.01, 0.001\}$ . We also show the best-tuned results in Figures A.12. From the figures, RASA-LR yields slightly better performance than others on the training MSE. All the algorithms converge to the same test MSE.

### B.5 Results for Algorithm A.1 (variable $\beta$ )

This section evaluates the performances of Algorithm A.1 by comparing it with RASA-LR of Algorithm 1 on the PCA problem with synthetic datasets. Figures A.13 (a) and (b) show all the results for different initial step size choices  $\alpha_0 = \{0.5, 0.1, 0.05, 0.01\}$  under well-conditioned and ill-conditioned cases, which correspond to Figures A.2 and A.3, respectively. From the figures, in both the cases, Algorithm A.1 is comparable to RASA-LR. However, the best result of Algorithm A.1 is slightly inferior to that of RASA-LR. In addition, it should be emphasized that Algorithm A.1 is computationally more inefficient than RASA as explained in Section A.4.

## C Manifolds

**Stiefel manifold**  $\text{St}(r, n)$ : The Stiefel manifold is the set of orthogonal  $r$ -frames in  $\mathbb{R}^n$  for some  $r \leq n$ , and it is an embedded submanifold of  $\mathbb{R}^{n \times r}$ . The orthogonal group  $O(n)$  is a special case of the Stiefel manifold, i.e.,  $O(n) = \text{St}(n, n)$ . Because  $\text{St}(r, n)$  is a submanifold embedded in  $\mathbb{R}^{n \times r}$ , we can endow the canonical inner product in  $\mathbb{R}^{n \times r}$  as a Riemannian metric  $\langle \xi, \eta \rangle_{\mathbf{U}} = \text{tr}(\xi^\top \eta)$  for  $\xi, \eta \in T_{\mathbf{U}}\text{St}(r, n)$ . With this Riemannian metric, the projection onto the tangent space  $T_{\mathbf{U}}\text{St}(r, n)$  is defined as an orthogonal projection  $\text{P}_{\mathbf{U}}(\mathbf{W}) = \mathbf{W} - \mathbf{U}\text{sym}(\mathbf{U}^\top \mathbf{W})$  for  $\mathbf{U} \in \text{St}(r, n)$  and  $\mathbf{W} \in \mathbb{R}^{n \times r}$ . A popular retraction is  $R_{\mathbf{U}}(\xi) = \text{qf}(\mathbf{U} + \xi)$  for  $\mathbf{U} \in \text{St}(r, n)$  and  $\xi \in T_{\mathbf{U}}\text{St}(r, n)$ , where  $\text{qf}(\cdot)$  extracts the orthonormal factor based on QR decomposition. Other details about optimization-related notions on the Stiefel manifold are in (Absil et al., 2008).

**Grassmann manifold**  $\text{Gr}(r, n)$ : A point on the Grassmann manifold is an equivalence class represented by a  $n \times r$  orthogonal matrix  $\mathbf{U}$  with orthonormal columns, i.e.,  $\mathbf{U}^\top \mathbf{U} = \mathbf{I}$ . Two orthogonal matrices express the same element on the Grassmann manifold if they are related by right multiplication of an  $r \times r$  orthogonal matrix  $\mathbf{O} \in O(r)$ . Equivalently, an element of  $\text{Gr}(r, n)$  is identified with a set of  $n \times r$  orthogonal matrices  $[\mathbf{U}] := \{\mathbf{U}\mathbf{O} : \mathbf{O} \in O(r)\}$ . That is,  $\text{Gr}(r, n) := \text{St}(r, n)/O(r)$ , where  $\text{St}(r, n)$  is the *Stiefel manifold* that is the set of matrices of size  $n \times r$  with orthonormal columns. The Grassmann manifold has the structure of a Riemannian quotient manifold (Absil et al., 2008, Section 3.4). A popular retraction on the Grassmann manifold is  $R_{\mathbf{U}}(\xi) = \text{qf}(\mathbf{U} + \xi)$ . Other details about optimization-related notions on the Grassmann manifold are in (Absil et al., 2008).

## D Problems and derivations of the Riemannian gradient

**ICA problem** (Theis et al., 2009): A particular variant to solve the independent components analysis (ICA) problem is through joint diagonalization on the Stiefel manifold, i.e.,

$$\min_{\mathbf{U} \in \mathbb{R}^{n \times r}} f_{\text{ica}}(\mathbf{U}) := -\frac{1}{N} \sum_{i=1}^N \|\text{diag}(\mathbf{U}^\top \mathbf{C}_i \mathbf{U})\|_F^2,$$

where  $\|\text{diag}(\mathbf{A})\|_F^2$  defines the sum of the squared diagonal elements of  $\mathbf{A}$ .  $\mathbf{C}_i$  can, for example, be cumulant matrices or time-lagged covariance matrices of size  $n \times n$ . The Riemannian gradient  $\text{grad}f_{\text{ica}}(\mathbf{U})$  of the cost function  $f_{\text{ica}}(\mathbf{U})$  is

$$\text{grad}f_{\text{ica}}(\mathbf{U}) = \text{P}_{\mathbf{U}}(\text{egrad}f_{\text{ica}}(\mathbf{U})) = \text{P}_{\mathbf{U}}\left(-\frac{1}{N} \sum_{i=1}^N 4\mathbf{C}_i \mathbf{U} \text{ddiag}(\mathbf{U}^\top \mathbf{C}_i \mathbf{U})\right),$$

where  $\text{egrad}f_{\text{ica}}(\mathbf{U})$  is the Euclidean gradient of  $f_{\text{ica}}(\mathbf{U})$ ,  $\text{ddiag}$  is the diagonal matrix, and  $\text{P}_{\mathbf{U}}$  denotes the orthogonal projection onto the tangent space of  $\mathbf{U}$ , i.e.,  $T_{\mathbf{U}}\text{St}(r, n)$ , which is defined as  $\text{P}_{\mathbf{U}}(\mathbf{W}) = \mathbf{W} - \mathbf{U}\text{sym}(\mathbf{U}^\top \mathbf{W})$ , where  $\text{sym}(\mathbf{A})$  represents the symmetric matrix  $(\mathbf{A} + \mathbf{A}^\top)/2$ .

**PCA problem:** Given an orthonormal matrix projector  $\mathbf{U} \in \text{St}(r, n)$ , which is the Stiefel manifold that is the set of matrices of size  $n \times r$  with orthonormal columns, the principal components analysis (PCA) problem is to minimize the sum of squared residual errors between projected data points and the original data as

$$\min_{\mathbf{U} \in \text{St}(r, n)} \frac{1}{N} \sum_{i=1}^N \|\mathbf{z}_i - \mathbf{U}\mathbf{U}^\top \mathbf{z}_i\|_2^2,$$

where  $\mathbf{z}_i$  is a data vector of size  $n \times 1$ . This problem is equivalent to

$$\min_{\mathbf{U} \in \text{St}(r, n)} f_{\text{pca}}(\mathbf{U}) := -\frac{1}{N} \sum_{i=1}^N \mathbf{z}_i^\top \mathbf{U} \mathbf{U}^\top \mathbf{z}_i.$$

Similar to the arguments in the ICA problem above, the expressions of the Riemannian gradient for the PCA problem on the Grassmann manifold is as follows:

$$\text{grad} f_{\text{pca}}(\mathbf{U}) = \mathbf{P}_{\mathbf{U}} (\text{egrad} f_{\text{pca}}(\mathbf{U})) = \mathbf{P}_{\mathbf{U}} \left( -\frac{1}{N} \sum_{i=1}^N 2\mathbf{z}_i \mathbf{z}_i^\top \mathbf{U} \right),$$

where the orthogonal projector  $\mathbf{P}_{\mathbf{U}}(\mathbf{W}) = \mathbf{W} - \mathbf{U} \mathbf{U}^\top \mathbf{W}$ .

**MC problem:** The matrix completion (MC) problem amounts to completing an incomplete matrix  $\mathbf{Z}$ , say of size  $n \times N$ , from a small number of entries by assuming a low-rank model for the matrix. If  $\Omega$  is the set of the indices for which we know the entries in  $\mathbf{Z}$ , the rank- $r$  MC problem amounts to solving the problem

$$\min_{\mathbf{U} \in \mathbb{R}^{n \times r}, \mathbf{A} \in \mathbb{R}^{r \times N}} \|(\mathbf{U} \mathbf{A})_{\Omega} - \mathbf{Z}_{\Omega}\|_F^2,$$

where  $\Omega$  is the set of indices whose entries are known. Partitioning  $\mathbf{Z} = [\mathbf{z}_1, \mathbf{z}_2, \dots, \mathbf{z}_N]$ , the problem is equivalent to the problem

$$\min_{\mathbf{U} \in \mathbb{R}^{n \times r}, \mathbf{a}_i \in \mathbb{R}^r} \frac{1}{N} \sum_{i=1}^N \|(\mathbf{U} \mathbf{a}_i)_{\Omega_i} - \mathbf{z}_{i\Omega_i}\|_2^2,$$

where  $\mathbf{z}_i \in \mathbb{R}^n$  and  $\Omega_i$  is the set of indices (of known entries) for the  $i$ -th column. Given  $\mathbf{U}$ ,  $\mathbf{a}_i$  admits the closed-form solution  $a_i = \mathbf{U}_{\Omega_i}^\dagger \mathbf{z}_{i\Omega_i}$ , where  $\dagger$  is the pseudo inverse and  $\mathbf{U}_{\Omega_i}$  and  $\mathbf{z}_{i\Omega_i}$  are respectively the rows of  $\mathbf{U}$  and  $\mathbf{z}_i$  corresponding to the row indices in  $\Omega_i$ . Consequently, the problem only depends on the column space of  $\mathbf{U}$  and is on the Grassmann manifold (Boumal & Absil, 2015a), i.e.,

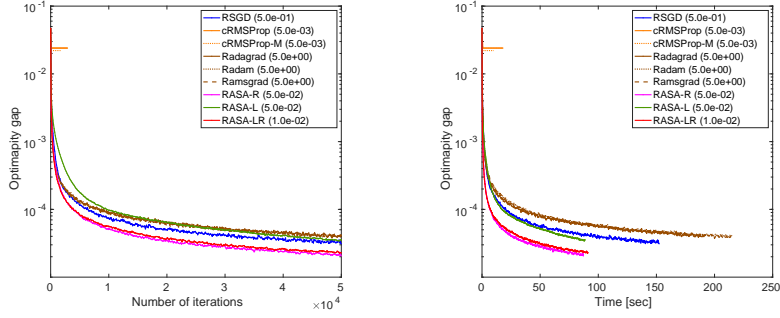
$$\min_{\mathbf{U} \in \text{Gr}(r, n)} f_{\text{mc}}(\mathbf{U}) := \min_{\mathbf{a}_i \in \mathbb{R}^r} \frac{1}{N} \sum_{i=1}^N \|(\mathbf{U} \mathbf{a}_i)_{\Omega_i} - \mathbf{z}_{i\Omega_i}\|_2^2.$$

The expressions of the Riemannian gradient for the MC problem on the Grassmann manifold is as follows:

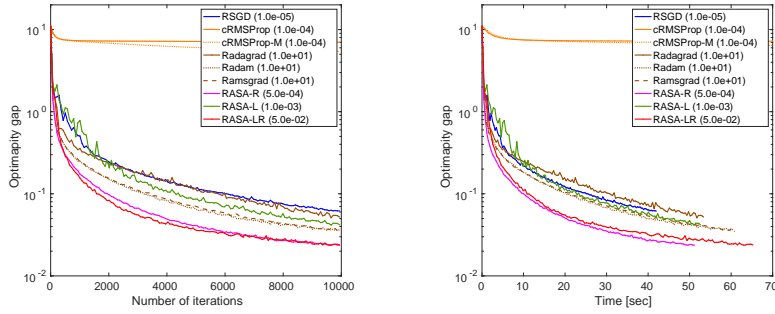
$$\text{grad} f_{\text{mc}}(\mathbf{U}) = \mathbf{P}_{\mathbf{U}} (\text{egrad} f_{\text{mc}}(\mathbf{U})) = \mathbf{P}_{\mathbf{U}} \left( \frac{1}{N} \sum_{i=1}^N 2((\mathbf{U} \mathbf{a}_i)_{\Omega_i} - \mathbf{z}_{i\Omega_i}) \mathbf{a}_i^\top \right),$$

where the orthogonal projector  $\mathbf{P}_{\mathbf{U}}(\mathbf{W}) = \mathbf{W} - \mathbf{U} \mathbf{U}^\top \mathbf{W}$ .

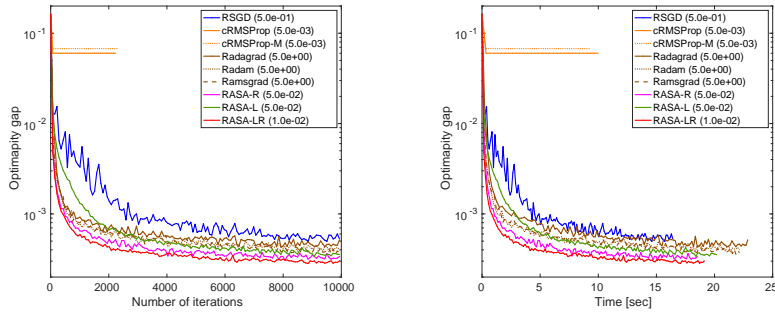




(a-1) Number of iterations. (a-2) Run-time.  
**(a) MNIST dataset (Case P2).**



(b-1) Number of iterations. (b-2) Run-time.  
**(b) COIL100 dataset (Case P3).**



(c-1) Number of iterations. (c-2) Run-time.  
**(c) COIL20 dataset.**

Figure A.4: Best-tuned results of real-world datasets on the PCA problem.

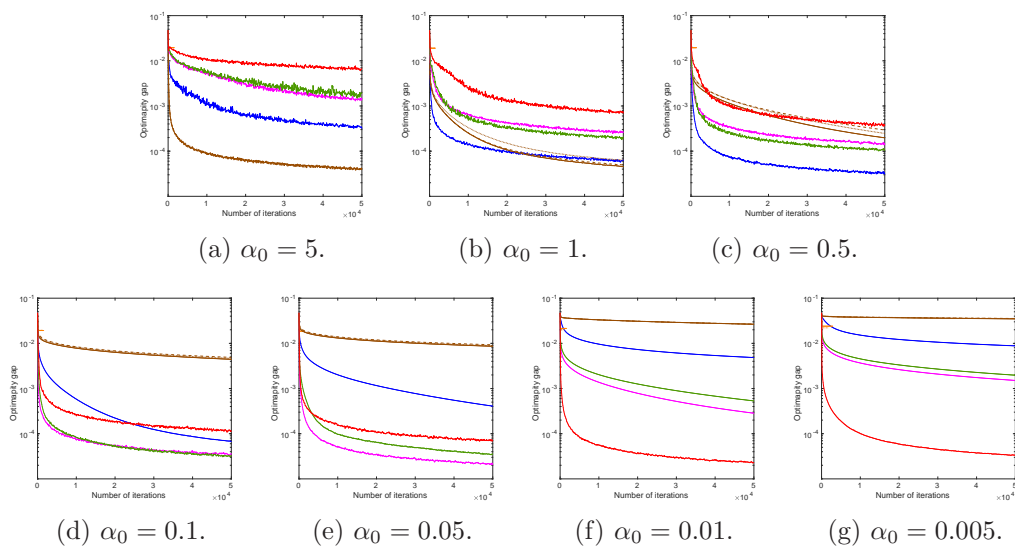


Figure A.5: MNIST dataset on the PCA problem (**Case P2**).

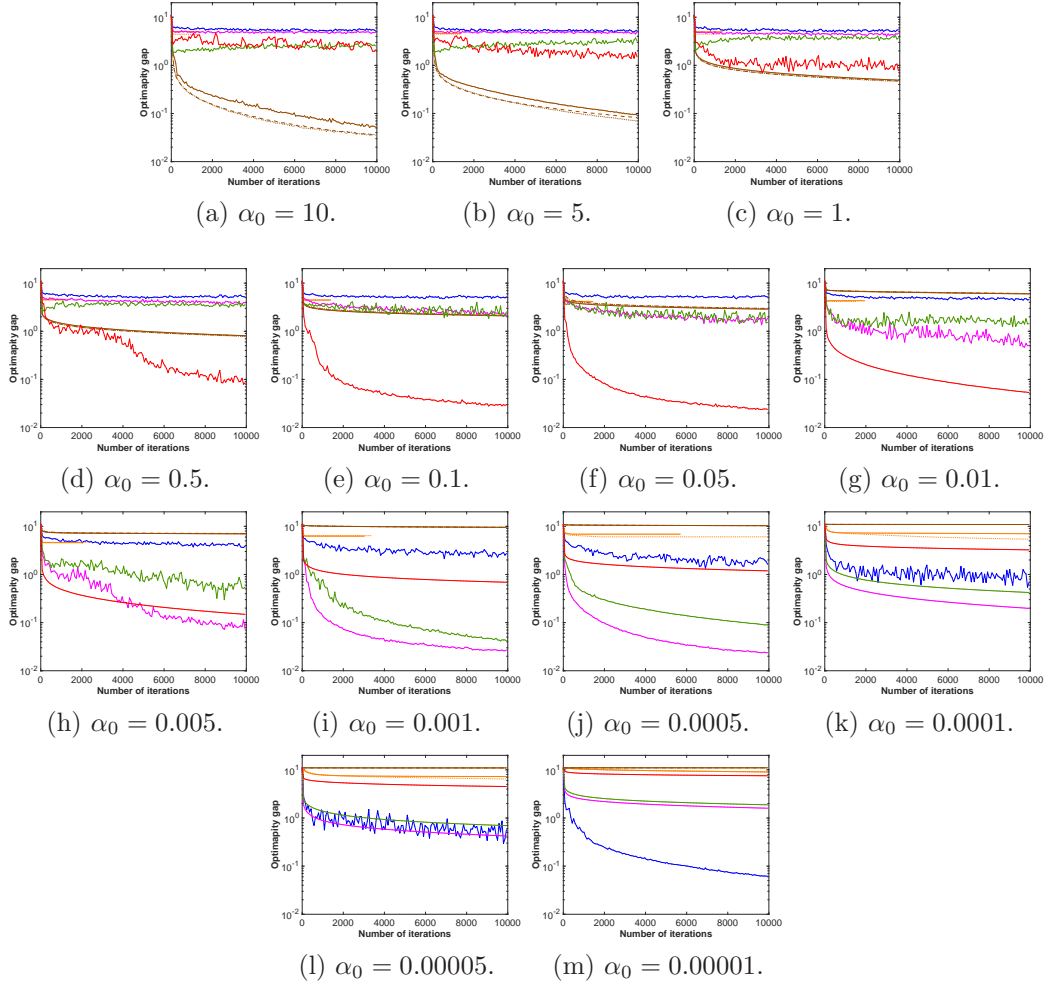


Figure A.6: COIL100 dataset on the PCA problem (**Case P3**).

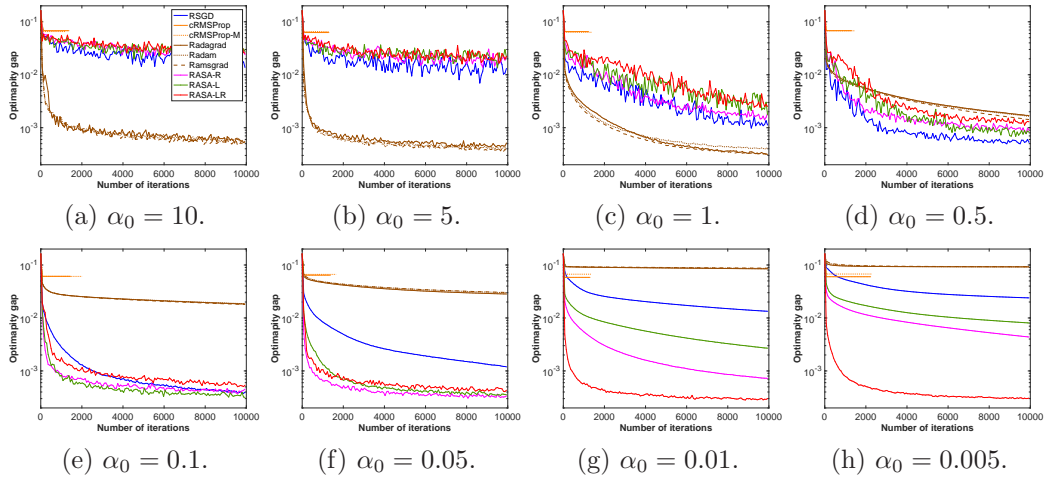


Figure A.7: COIL20 dataset on the PCA problem.

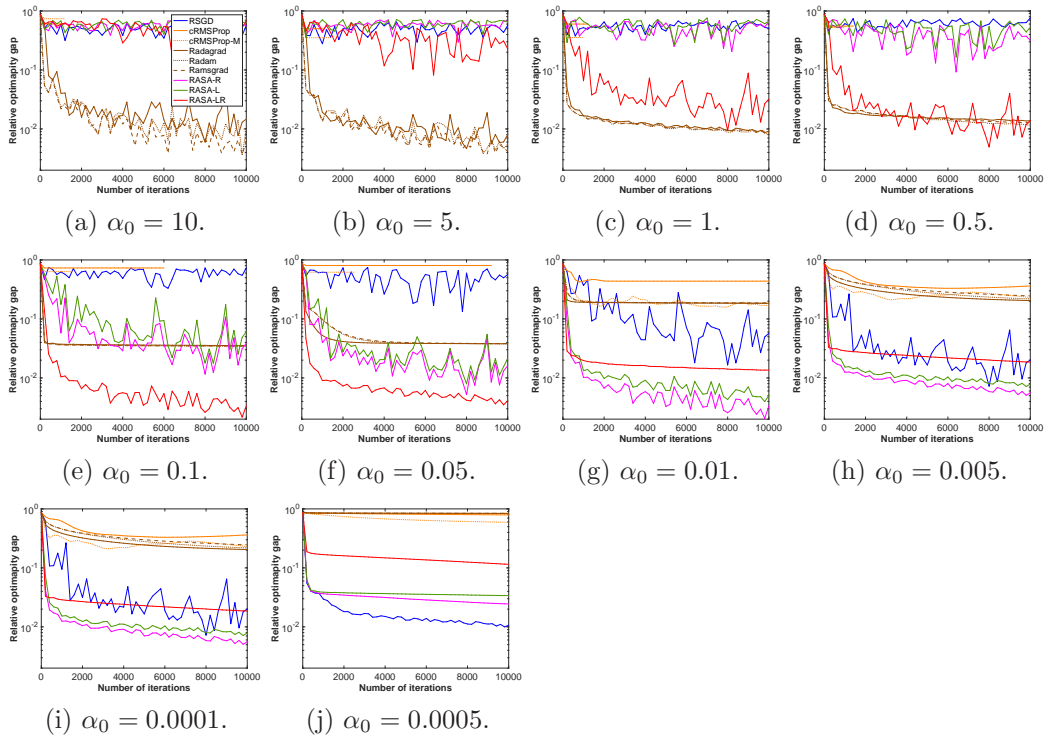


Figure A.8: YaleB dataset on ICA problem (Case I1).

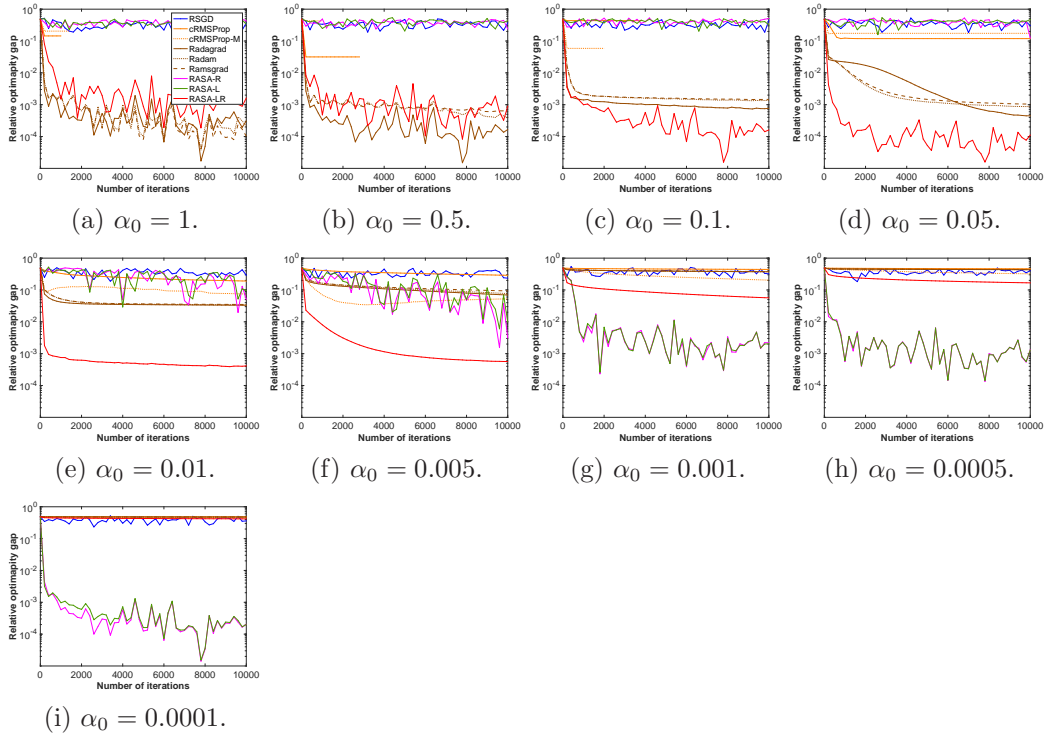
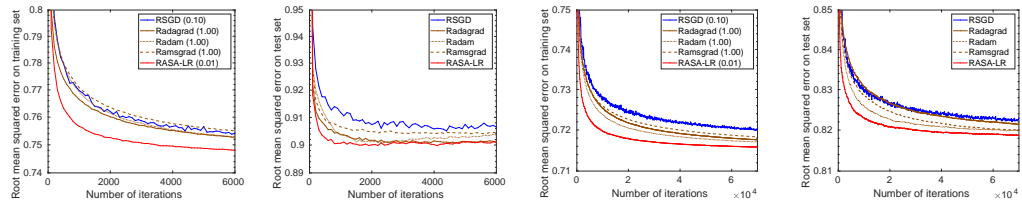


Figure A.9: COIL100 dataset for the ICA problem (**Case I2**).



(a) MovieLens-1M dataset.

(b) MovieLens-10M dataset.

Figure A.10: Best-tuned results of MovieLens dataset on MC problem.

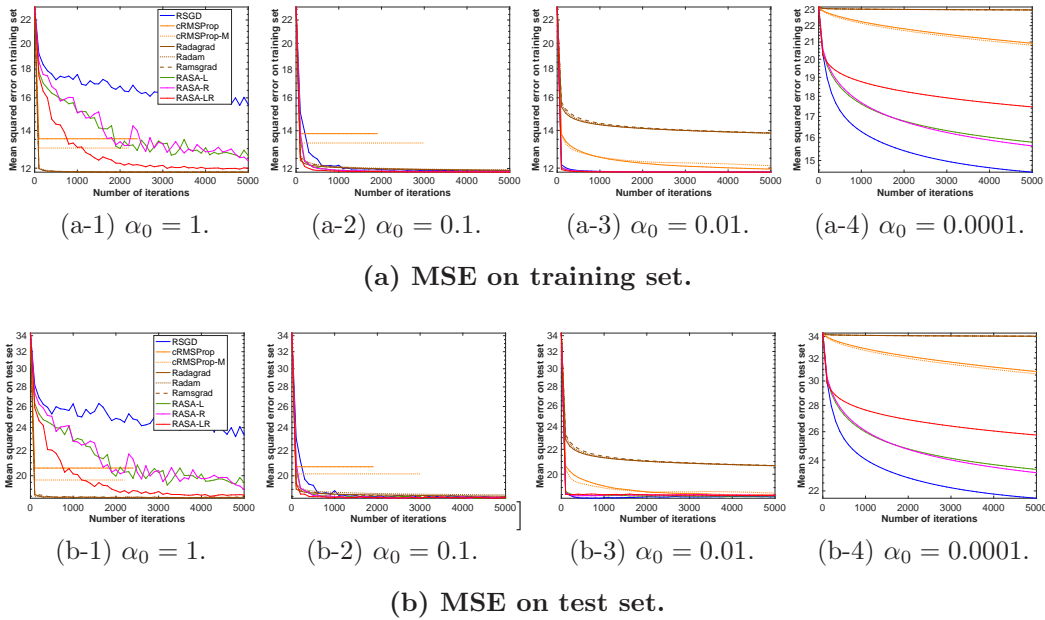


Figure A.11: Jester dataset for the MC problem.

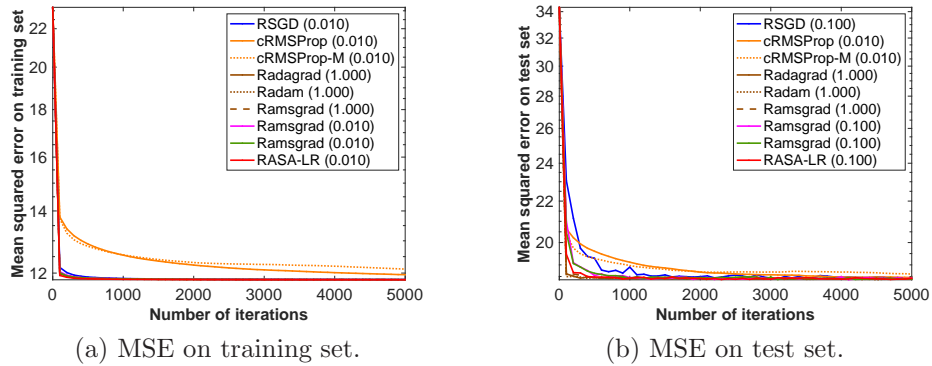


Figure A.12: Best-tuned results on the Jester dataset for the MC problem.

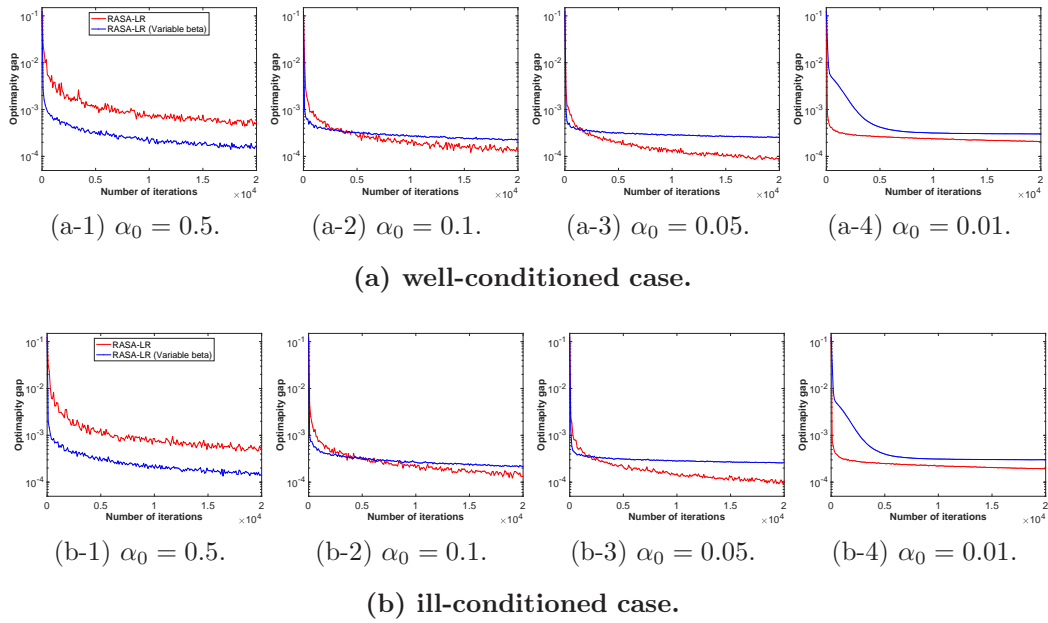


Figure A.13: Comparison between Algorithms 1 and A.1 on synthetic datasets for the PCA problem (Case P1).